Hybrid Channel Tracking for THz Massive MIMO Communication Systems in Dynamic Environments

Yuheng Fan, Chuang Yang, *Member, IEEE,* Yanran Sun, and Mugen Peng, *Fellow, IEEE*

***Abstract*—With gigahertz-level bandwidth, terahertz (THz) holds promise for achieving exceptionally high transmission rates in prospective sixth-generation (6G) communications. However, considerable loss poses an obstacle to THz communication. To compensate for this, massive multiple-input-multiple-output (MIMO) based beamforming is utilized to promote directional power with narrow beams in communication. In dynamic environments, the frequent adjustment of narrow beams results in fast time-varying channel state information (CSI), which constrains the application of the THz communication systems. While traditional deterministic-based and statistical-based channel tracking methods address different aspects of this issue, they suffer from balancing accuracy and complexity in the THz dynamic environments. To solve this problem, based on the cluster distribution of THz time-varying channel, we propose a novel hybrid channel tracking method that uses deterministic physical motion variation law to extract the cluster subspace, and then statistical Markov evolution models are applied within it. To achieve this, an integrated clustering and estimation method, clustering subspace matching pursuit (CSMP) is proposed for obtaining the channel clusters prior. Then based on above hybrid tracking method design, we propose a virtual cluster subspace turbo-approximate message passing (VCS-TAMP). Finally, several simulation results validate that our proposal achieves great improvement in both accuracy and computational time performance.**

***Index Terms*—Terahertz, massive MIMO, channel tracking.**

I. Introduction

TERAHERTZ (THz) band, spanning from 0.1 THz to 10 THz, offers gigahertz-level bandwidth to support massive connectivity [1], ultimate wireless virtual reality (VR) [2] and other huge-capacity demanded applications in envisioned sixth-generation (6G) communication [3]. Despite its bandwidth potential, THz communications still face severe path loss challenges due to its high-frequency loss and atmospheric absorption in air [4]. Based on massive MIMO systems, beamforming technologies have been widely employed to enhance THz directional transmission gain and compensate for the path loss [5], [6]. However, beamforming makes the THz beam much narrower than ever [7], leading to frequent adjustments to align with moving users in dynamic environments. This rapid beam change results in channel state information (CSI) fast time-varying [8], which presents challenges for reliable demodulation in THz communication. To solve this problem, a dynamic CSI prediction technology named channel tracking has been proposed nowadays [9]. Channel tracking methods usually comprise two primary phases, initialization and tracking. Initialization mirrors static channel estimation, establishing priors for subsequent tracking. In the latter tracking phase, the temporal correlation priors are applied to design relative algorithms. With these dynamic prior, channel tracking methods can significantly enhance accuracy and reduce computational overhead compared to static channel estimation [10]–[12]. Considering the accuracy and computation time requirement in THz dynamic environments, channel tracking has been a key technology to unlocking the vast spectrum resource for THz massive MIMO communication [13].

This work was supported by the National Key Research and Development Program of China under Grant 2021YFB2900200, in part by the Beijing Natural Science Foundation under grant L223007, in part by the National Natural Science Foundation of China under Grant 61925101, and 62101059. *(Corresponding author: Chuang Yang).*

Yuheng Fan, Chuang Yang, Yanran Sun, and Mugen Peng are with the State Key Laboratory of Networking and Switching Technology, Beijing University of Posts and Telecommunications, Beijing 100876, China (email: vanyh@bupt.edu.cn; chuangyang@bupt.edu.cn; sunyanran@bupt.edu.cn; pmg@bupt.edu.cn).

Manuscript received March xx, 2024; revised xxxxxxxxxxx.

A. Literature Review

As research progresses, channel tracking studies can be categorized into two main methods based on their different channel evolution models to predict the channel: statistical tracking (ST) methods employing Markov models, and deterministic tracking (DT) methods utilizing physical models.

For statistical tracking methods, the THz time-varying channel in dynamic environments is described by the Markov process model and then tracked through some prior information-modified algorithms [14], [15]. These methods commonly predict the channel itself and require minimal environmental information, which exhibits strong generalization capabilities. Reference [16] introduced a two-dimensional Markov model (2D-MM) to capture the joint time-space sparsity channel, and a dynamic turbo-orthogonal approximate message passing (D-TOAMP) algorithm was proposed for channel tracking. Reference [17], [18] extended 2D-MM to 3D on/off-grid space considering both azimuth and elevation. Besides, it also proposed relative 3D-dynamic turbo-AMP (3D-DTAMP) to track the dynamic channels. Though the above statistical channel tracking methods can achieve extremely high accuracy performance, they treated the transition probabilities as constants under the steady Markov transition assumption, which may no longer hold in THz time-varying channel [19], [20]. Especially in dynamic environments mixed with both line-of-sight (LoS) and non-line-of-sight (NLoS), even neighboring time slots may feature vastly different channels, posing challenges for computation time and even convergence.

The deterministic tracking (DT) method considers the channel as a deterministic signal well-defined by the environment.

This method extracts relevant practical parameters from the received signal and tracks them with electromagnetic and kinematic equations. Reference [21] focused on LoS condition in THz communication and proposed an angular iterative equation to aid channel tracking. Reference [22] considered NLoS paths as well. Reference [22] utilized the mirror temporal correlation to simplify the dynamic AoA variation law on scattering NLoS path tracking. In a more grand scene, reference [23] proposed an iterative angle and Doppler channel tracking variation law in space-air-ground integrated THz networks. Although the above methods have achieved improvements in time consumption performance while ensuring acceptable accuracy, tracking the channel through AoA, delay, and other physical parameters ignores some more complex features such as scattering, rotation, and vibrations, which is the reason for their limited tracking accuracy performance. Moreover, this method relies highly on the environment prior, such as LoS only [21], the known motion [22], [24], navigation prior [23]. Without matched priors in the THz dynamic environments, these methods usually had accuracy degradation.

In summary, traditional channel tracking methods struggle to strike a balance between accuracy and time computation in the context of practical THz massive MIMO communication systems. To the best of our knowledge, the channel tracking for THz massive MIMO communication systems in dynamic environments has not been well addressed so far.

B. Motivation and Contribution

To address this issue, exploring the underlying prior information within the THz channel is crucial. In the geometry-based statistical model (GBSM), THz channels are split into inter-cluster and intra-cluster two part [25], [26], modeled using deterministic ray tracing and distribution generation techniques respectively. Therefore, GBSM offers a precise description of THz channels with minimal parameters. Inspired by this, we attempt to combine ST and DT into a hybrid one. However, developing the Hybrid Tracking (HT) method poses some new challenges, and our main work and contributions are summarized as follows:

1) To integrate the Markov channel evolution model with the physical one, we introduce a novel hybrid channel evolution model to capture the THz time-varying channels. Through clustered CSI, the channel is modeled using hidden support and value vectors. The channel support is divided into different parts. Deterministic support, whose evolution model is derived from ray modeling and kinematics equations, extends to form subspace channels. In the subspace, statistical evolution modeling, employing a Markov process, captures complex motion and scattering phenomena, robustly representing channel variations. And simulation also shows our proposed channel variation model owns a much lower outage probability under perfect CSI.
2) To solve the problem of obtaining the above-mentioned deterministic supports, we propose a clustering subspace matching pursuit (CSMP) to obtain the clustered CSI in initialization. As traditional estimation methods struggle to acquire clustered CSI effectively, leading to inaccurate clustered CSI for later tracking phase. Through computing cluster residuals to select atoms, CSMP integrates both channel estimation and clustering so that the channel label and value are estimated simultaneously. The simulation result also supports that our proposal improves both estimation and clustering performance compared with traditional methods.
3) To enhance channel tracking performance while minimizing time consumption for THz massive MIMO communication systems, we devise a virtual cluster subspace-turbo orthogonal approximate message passing (VCS-TAMP) algorithm. The VCS-TAMP approach conducts parallel processing across subspace channels. This strategy not only reduces problem complexity to the subspace within each cluster but also improves tracking accuracy based on more consistent channel characteristics within clusters.

In contrast to the aforementioned contributions, the remaining sections of this paper have been reorganized for clarity and simplicity. In section II, we first introduce our communication model. Then hybrid channel evolution model is introduced in section III. The hybrid channel tracking scheme and relative algorithms are described in section IV. Several simulations and numeric validation results are presented in section V. Finally, our work is summarized in section VI.

Notation: In this paper, bold uppercase and lowercase letters stand for matrices and vectors, respectively. Superscripts $(\mathbf{X})^T$, $(\mathbf{X})^H$, $(\mathbf{X})^{-1}$ denote the transposition, Hermitian and inverse of $\mathbf{X}$. The vector version of a matrix is noted as vec, obtained by stacking columns into a single-column vector, whose reverse process is $devec$. Estimation of $(\mathbf{X})$ is denoted as $(\hat{\mathbf{X}})$. The symbol $\otimes$ stands for the Kronecker product of two matrices.

II. SYSTEMS MODEL

In this paper, we consider a typical uplink tracking process between single-antenna users and the base station (BS) equipped with an N_r-antenna uniform linear array (ULA) within an N_s-symbol time slot in orthogonal frequency division multiplex (OFDM) system. With orthogonal symbols, our following analysis focuses on one specific user. When the user transmits orthogonal symbols vector $\mathbf{x} \in \mathbb{C}^{N_s \times 1}$ to the BS, the received signal $\mathbf{Y} \in \mathbb{C}^{N_{RF} \times N_s}$ is expressed as:

$$\mathbf{Y} = \mathbf{W}\mathbf{h}\mathbf{x}^T + \mathbf{W}\mathbf{n}, \tag{1}$$

where $\mathbf{W} \in \mathbb{C}^{N_{RF} \times N_r}$ is BS combining matrix, $\mathbf{h} \in \mathbb{C}^{N_r \times 1}$ is THz channel vector, $\mathbf{n} \in \mathbb{C}^{N_r \times N_s}$ is addictive Gaussian white noise matrix. According to the propagation model in reference [25], [26], the channel $\mathbf{h}$ is formulated as:

$$\mathbf{h} = \sum_{i=1}^{N_i} \sum_{l=1}^{N_{li}} g_{i,l} \boldsymbol{\alpha}(\theta_{i,l}) e^{-j2\pi f_m \tau_{i,l}}, \tag{2}$$

where f_m represents subcarrier spacing, parameters $g_{i,l}, \tau_{i,l}, \theta_{i,l}$ are channel gain, delay, and AoA of l-th path within ith cluster respectively. When antenna unit

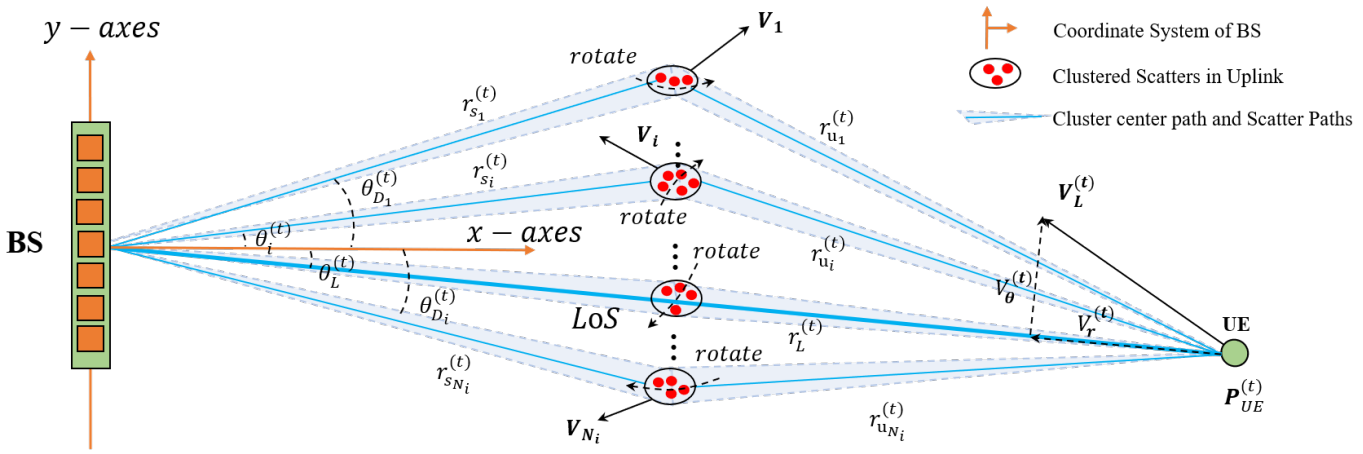

Fig. 1. Uplink channel tracking procedure of THz massive MIMO communication systems in dynamic environments.

spacing is set at half-wavelength, the steering vector $\boldsymbol{\alpha}(\theta)$ is as:

$$\boldsymbol{\alpha}(\theta) = \left[1, e^{-j\pi \sin\theta} \cdots, e^{-j(N_r-1)\pi \sin\theta}\right]. \tag{3}$$

To better illustrate the tracking problem in the following parts, equation (1) is reformulated into :

$$\mathbf{y} = (\mathbf{W}\mathbf{h}) \otimes \mathbf{X} + \tilde{\mathbf{n}} = (\mathbf{W} \otimes \mathbf{X})\,\mathbf{h} + \tilde{\mathbf{n}}, \tag{4}$$

where $\mathbf{y} = vec(\mathbf{Y})$, and $\tilde{\mathbf{n}} = vec(\mathbf{W}\mathbf{n})$ and $\mathbf{h}$ is the vector to be estimated. Due to THz narrow beams and the high path loss, the THz channel shows inherent joint sparsity on the delay-angular (DA) domain of THz massive MIMO channels [27]. Sparse channel $\tilde{\mathbf{h}} \in \mathbb{C}^{N_r N_s \times 1}$ is obtained using the transformation:

$$\mathbf{h} = (\mathbf{F}_{N_r} \otimes \mathbf{\Pi}_{N_s})\tilde{\mathbf{h}}, \tag{5}$$

where $\mathbf{F}_{N_r} \in \mathbb{C}^{N_r \times N_r}$ is a N_r-order discrete fourier transform (DFT) matrix, $\mathbf{\Pi} = \left[1, \cdots, e^{-j2\pi f_m \tau_{N_s}}\right]$ is $1 \times N_s$-size delay transform vector and $\tau_m = m/B$ with B denoting the total bandwidth in THz communication systems.

Considering different time slots, the estimation problem in equation (4) can be extended to the sparse channel tracking problem as:

$$\mathbf{y}^{(t)} = \mathbf{\Phi}\tilde{\mathbf{h}}^{(t)} + \tilde{\mathbf{n}}, \tag{6}$$

where $\mathbf{\Phi} = (\mathbf{W} \otimes \mathbf{X})\,(\mathbf{F}_{N_r} \otimes \mathbf{\Pi}_{N_s}) = (\mathbf{W}\mathbf{F}_{N_r}) \otimes (\mathbf{X}\mathbf{\Pi}_{N_s})$ is transformation measurement matrix. Because $N_{RF} \ll N_r$ always holds in THz massive MIMO communication systems, recovery of sparse channel vector is a typical compressed sensing (CS) problem. Therefore, we aimed to obtain a robust estimation of the time-varying channel $\tilde{\mathbf{h}}^{(t)}$ through CS estimation technologies with some prior passed from previous time slots in this paper.

III. The Hybrid Channel Evolution Model

To capture the time-varying THz channel in dynamic environments, we present a hybrid channel evolution model consisting of four key components: subspace channel establishment, deterministic evolution modeling, subspace statistical support evolution modeling, and value evolution modeling.

A. Establishment of subspace channels

we arrange the highest-power center path channel support of each cluster as deterministic support vector $\mathbf{\Omega}^{(t)}$, whose element is a 2D array (m_i, n_i). The i-th element in the deterministic support vector is determined by:

$$\mathbf{\Omega}^{(t)}(i) = \left(mod(I_{i,L}^{(t)}, N_s), mod(I_{i,L}^{(t)}/N_s, N_r)\right). \tag{7}$$

Given the cluster distribution characteristics of THz time-varying channel, other paths within the i-th cluster are situated in a 2D subspace $\mathbf{S}_i^{(t)}$ around the center $\mathbf{\Omega}^{(t)}(i)$, with delay and AoA expanding grid numbers ϵ_τ and ϵ_θ as Fig.2. Therefore, we can construct a subspace for i-th cluster channel as:

$$\mathbf{h}_i^{(t)} = \tilde{\mathbf{h}}^{(t)}(\mathbf{S}_i) \tag{8}$$

The subspace channel $\mathbf{h}_i^{(t)}$ is modeled through hidden support vector $\mathbf{b}_i^{(t)}$ and hidden value vector $\mathbf{v}_i^{(t)}$ as [15]:

$$\mathbf{h}_i^{(t)} = \mathbf{b}_i^{(t)} \cdot \mathbf{v}_i^{(t)}, \tag{9}$$

The subspace channel joint probability distribution is as follows:

$$p\left(\mathbf{h}_i^{(t)}, \mathbf{b}_i^{(t)}, \mathbf{v}_i^{(t)}\right) = p\left(\mathbf{h}_i^{(t)} | \mathbf{b}_i^{(t)}, \mathbf{v}_i^{(t)}\right) p\left(\mathbf{b}_i^{(t)}\right) p\left(\mathbf{v}_i^{(t)}\right), \tag{10}$$

where the conditional prior channel vector is:

$$p\left(\mathbf{h}_i^{(t)} | \mathbf{b}_i^{(t)}, \mathbf{v}_i^{(t)}\right) = \prod_{t=1}^{T} \delta\left(\mathbf{h}_i^{(t)} - \mathbf{b}_i^{(t)} \cdot \mathbf{v}_i^{(t)}\right). \tag{11}$$

Therefore, the whole channel evolution model concludes three parts $\mathbf{\Omega}^{(t)}$, $p\left(\mathbf{b}_i^{(t)}\right)$ and $p\left(\mathbf{v}_i^{(t)}\right)$ for subspace channel, which is introduced in following parts.

B. Deterministic Support Evolution Model

Physical parameter $[r_i^{(t)}, \theta_i^{(t)}]^T$ on channel is derived through the on-grid deterministic channel characteristics as:

$$\begin{cases} r_i^{(t)} = \Delta\lambda \cdot m_i \\ \theta_i^{(t)} = sin^{-1}(\Delta\omega \cdot n_i) \end{cases}, (m_i, n_i) \in \mathbf{\Omega}^{(t)}, \tag{12}$$

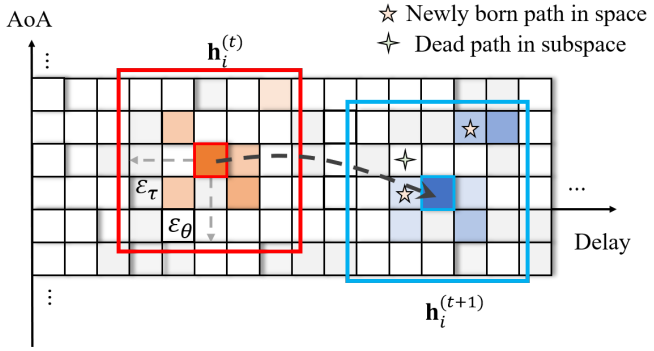

Fig. 2. Subspace channel variation in consecutive time slots.

where $\Delta\omega = 1/N_r$ is the normalized angle spacing, $\Delta\lambda = C/B$ is the wavelength spacing with light speed C. As the analysis of NLoS scenarios is considerably more complex, in the following parts, we will initially introduce the evolution model LoS channels and then discuss how to incorporate NLoS considerations into the LoS framework. The entire process is illustrated in Algorithm 1.

1) LOS condition: Because the LoS channel directly links the BS and users, the physical location of the user $\mathbf{P}_u^{(t)}$ in the rectangular coordinate systems is promptly derived from the motion state of the LoS channel:

$$\mathbf{P}_u^{(t)} = \left(r_L^{(t)}\cos\theta_L^{(t)}, r_L^{(t)}\sin\theta_L^{(t)}\right). \tag{13}$$

Thanks to THz ultra-wide bandwidth, moving of users between consecutive time slots can be as linear [21]. Current velocity is approximated as consecutive time difference as:

$$\mathbf{V}_L^{(t)} \approx \frac{1}{T}\left(\mathbf{P}_u^{(t)} - \mathbf{P}_u^{(t-1)}\right), \tag{14}$$

which can be decomposed by projecting on radial and tangential unit vectors as V_r and V_θ respectively. So the increment of relative distance and AoA is predicted as:

$$\begin{cases} \Delta r_L^{(t)} = r_L^{(t)} - r_L^{(t-1)}\cos\left(\theta_L^{(t)} - \theta_L^{(t-1)}\right), \\ \Delta\theta_L^{(t)} = \dfrac{r_L^{(t-1)}}{r_L^{(t)}}\sin\left(\theta_L^{(t)} - \theta_L^{(t-1)}\right). \end{cases} \tag{15}$$

Therefore, the variation and predicted result of main support is formulated as:

$$\hat{\mathbf{\Omega}}^{(t+1)}(L) = \left[\frac{r_L^{(t)} + \Delta r_L^{(t)}}{\Delta\lambda}, \frac{\sin\left(\theta_L^{(t)} + \Delta\theta_L^{(t)}\right)}{\Delta\omega}\right]. \tag{16}$$

2) NLOS condition: In Fig.1, NLoS channels distance $r_i^{(t)}$ are divided into $r_{s_i}^{(t)}$ and $r_{u_i}^{(t)}$ two parts by scatters. As user position has been predicted, we can use cosine theorem techniques to predict the scatter distance $\hat{r}_{s_i}^{(t+1)}$. With the obtained AoA angle equaling the scatterer physical angle, the relationship among distance $r_L^{(t)}$, $r_{s_i}^{(t)}$, and $r_{u_i}^{(t)}$ satisfy the cosine theorem as:

$$\left(r_{u_i}^{(t)}\right)^2 = \left(r_L^{(t)}\right)^2 + \left(r_{s_i}^{(t)}\right)^2 - 2r_L^{(t)}r_{s_i}^{(t)}\cos\theta_{D_i}, \tag{17}$$

Algorithm 1 Deterministic Support Evolution

INPUT: Deterministic channel support $\mathbf{\Omega}^{(t-1)}$, $\mathbf{\Omega}^{(t)}$.
OUTPUT: Predicted channel $\hat{\mathbf{\Omega}}^{(t+1)}$.
Transform channel motion state at time slot t and $t-1$ through equation(12).
For $i = 1 : N_i$
  If $i = L$ **Do:**
    Calculate $\Delta r_L^{(t)}, \Delta\theta_L^{(t)}$through (15).
    Predict $\hat{\mathbf{\Omega}}^{(t+1)}(L)$ through equation (16).
  Else % NLoS condition
    Calculate $r_{s_i}^{(t-1)}, r_{s_i}^{(t)}$ through (18).
    Update $[r_{s_i}^{(t)}, \theta_{s_i}^{(t)}]^T$ and $[r_{s_i}^{(t-1)}, \theta_{s_i}^{(t-1)}]^T$.
    Calculate $\Delta r_{s_i}^{(t)}, \Delta\theta_{s_i}^{(t)}$ through (15).
    $\hat{r}_{s_i}^{(t+1)} = r_{s_i}^{(t)} + \Delta r_{s_i}^{(t)}$.
    Calculating $\hat{r}_i^{(t+1)}$ through (19).
    $\hat{\theta}_i^{(t+1)} = \theta_i^{(t)} + \Delta\theta_{s_i}^{(t)}$.
    $\hat{\mathbf{\Omega}}^{(t+1)}(i) = \left(\dfrac{\hat{r}_i^{(t+1)}}{\Delta\lambda}, \dfrac{\sin\left(\hat{\theta}_i^{(t+1)}\right)}{\Delta\omega}\right)$.
  End If
End For

where $\theta_{D_i}^{(t)} = \theta_i^{(t)} - \theta_L^{(t)}$ is the AoA shift between LoS and i-th NLoS cluster center path. Substituting $r_{u_i}^{(t)} = r_i^{(t)} - r_{s_i}^{(t)}$ into equation (17), the calculated closed form of $r_{s_i}^{(t)}$ is as:

$$r_{s_i}^{(t)} = \frac{\left(r_i^{(t)}\right)^2 - \left(r_L^{(t)}\right)^2}{2r_i^{(t)} - r_L^{(t)}\cos\theta_{D_i}^{(t)}}. \tag{18}$$

After obtaining $r_{s_i}^{(t)}$, we determine the scatters' position. This scatterers' position is also predicted through equation (15). Then to get predicted CSI, we reintroduce the predicted scatter positions into (17) and predict $\hat{r}_i^{(t+1)}$ as:

$$\hat{r}_i^{(t+1)} = \hat{r}_{s_i}^{(t+1)}\left(1 + \sqrt{1 - 2\kappa_i^{(t+1)}\cos\theta_{D_i}^{(t+1)} + \left(\kappa_i^{(t+1)}\right)^2}\right), \tag{19}$$

where $\kappa_i^{(t+1)} = \hat{r}_L^{(t+1)}/\hat{r}_{s_i}^{(t+1)}$ is the user-scatterers distance ratio. After that, the predicted channel support is obtained and the complete deterministic support evolution model is summarized in Algorithm 1.

C. Subspace Statistical Evolution Model

As Fig.2 shown, cluster subspace hidden support $\mathbf{b}_i^{(t)}$ is the combination of delay and AoA, their joint channel support probability is given by

$$p\left(\mathbf{b}_i^{(t)}\right) = p\left(\mathbf{b}_i^{(t)}|\mathbf{d}_i^{(t)}, \mathbf{a}_i^{(t)}\right) p\left(\mathbf{d}_i^{(t)}\right) p\left(\mathbf{a}_i^{(t)}\right), \tag{20}$$

where $\mathbf{d}_i$, $\mathbf{a}_i$ are the delay and AoA support vector with ϵ_τ and ϵ_θ elements respectively. For the sake of simplicity, we make the vectors in the subsequent discussion can be indexed in this 2D support which satisfies:

$$\mathbf{b}^{(t,m,n)} = \mathbf{b}^{(t)}(m + (n-1)\times\epsilon_\tau). \tag{21}$$

And other relative subspace vector mentioned in the following section is presented similarly.

As the center path has been predicted by deterministic support, message passing starting from the central sub-path can speed up following the convergence of the algorithm. Our proposed subspace statistical support evolution model computes delay and AoA support probability from the central path to the marginal path as equation(22), where $\boldsymbol{\chi} \in \mathbb{C}^{\epsilon_\chi \times 1}$ can be either $\mathbf{d}_i \in \mathbb{C}^{\epsilon_\tau \times 1}$ or $\mathbf{a}_i \in \mathbb{C}^{\epsilon_\theta \times 1}$. And according to the reference [17], the conditional probability with known $\mathbf{d}_i^{(t,m)}, \mathbf{a}_i^{(t,n)}$ is given by:

$$p\left(\mathbf{b}_i^{(t,m,n)} | \mathbf{d}_i^{(t,m)}, \mathbf{a}_i^{(t,n)}\right) = \mathbf{d}_i^{(t,m)} \cdot \mathbf{a}_i^{(t,n)} \gamma^{\mathbf{b}_i^{(t,m,n)}} (1-\gamma)^{\mathbf{b}_i^{(t,m,n)}} + \left(1 - \mathbf{d}_i^{(t,m)} \mathbf{a}_i^{(t,n)}\right) \delta\left(\mathbf{b}_i^{(t,m,n)}\right), \tag{23}$$

where γ is a hyper-parameter determining the probability of the overall support vector supports when the independent delay and AoA supports.

D. Subspace Value Variation Law

It is crucial to not only model the channel support but also to track their value changes over time. Due to the complexities of the THz time-varying channel in dynamic environments, the distribution of values for different paths can be intricate. Therefore, we assume that hidden value elements within the subspace are independent but follow a Gaussian Markov process over time due to their smooth value change as:

$$\mathbf{v}_i^{(t+1)} = (1-\beta)\left(\mathbf{v}_i^{(t)} - \bar{\boldsymbol{\mu}}_i\right) + \beta w + \bar{\boldsymbol{\mu}}_i, \tag{24}$$

where $\bar{\boldsymbol{\mu}}_i$ represents the mean value, w is the noise, $\beta \in [0,1]$ is time related parameters.The formula has a mean value $\bar{\boldsymbol{\mu}}_i$, a complex Gaussian noise $w \sim \mathcal{CN}(0, \sigma_w^2)$, and a time-related parameter β that ranges from 0 to 1. When $\beta = 0$, the channel value is static. When $\beta = 1$, the channel follows the i.i.d. Gaussian distribution over time. For values of β between 0 and 1, the conditional probability is determined by formula:

$$p\left(\mathbf{v}_i^{(t+1)} | \mathbf{v}_i^{(t)}\right) \sim \mathcal{CN}(\mathbf{v}_i^{(t+1)}, (1-\beta)\mathbf{v}_i^{(t)} + \beta\bar{\boldsymbol{\mu}}_i, \beta^2\sigma_w^2). \tag{25}$$

Therefore, we have developed a hybrid channel evolution model based on our previous discussions. This model predicts the central path of each cluster deterministically and examines the subspace channel path changes through the probability distribution of hidden support vectors and value vectors within a subspace. In the upcoming section, we will provide a detailed overview of the hybrid channel tracking method based on this model.

Algorithm 2 Hybrid Channel Tracking

INPUT: $\left[\mathbf{y}^{(1)}, \cdots, \mathbf{y}^{(T)}\right]$, $\boldsymbol{\Phi}, N_c, \epsilon_\theta, \epsilon_\tau$.
OUTPUT: $\left[\hat{\mathbf{h}}^{(1)}, \cdots, \hat{\mathbf{h}}^{(T)}\right]$.

When $t \le t'$ % Initialization phase
  $\left[\hat{\mathbf{h}}^{(t)}, \hat{\boldsymbol{\Omega}}^{(t)}\right]$ = **CSMP** $\left(\mathbf{y}^{(t)}, \boldsymbol{\Phi}, N_c, \epsilon_\tau, \epsilon_\theta\right)$
End When

When $t \ge t'+1$ % Tracking phase
  Obtain $\hat{\boldsymbol{\Omega}}^{(t)}$ based on $\hat{\boldsymbol{\Omega}}^{(t-1)}, \hat{\boldsymbol{\Omega}}^{(t-2)}$ in **Algorithm 1**.
  For $i = 1 : N_i$
    $\mathbf{S}_i^{(t)} = (m_{i,1} - \epsilon_\tau : m_{i,1} + \epsilon_\tau, n_{i,1} - \epsilon_\theta : n_{i,1} + \epsilon_\theta)$.
    $\boldsymbol{\Phi}_i^{(t)} = \boldsymbol{\Phi}(:, m + (n-1) \times N_s), \quad (m,n) \in \mathbf{S}_i$
  End For
  Par-For $i = 1 : N_i$
    While not convergence **do**
      Update $\mathbf{h}_{i,\mathcal{A}_{post}}^{(t)}$ and $v_{i,\mathcal{A}_{post}}^{(t)}$ in (33).
      Update $\mathbf{h}_{i,\mathcal{A}_{ext}}^{(t)}$ and $v_{i,\mathcal{A}_{ext}}^{(t)}$ in (35).
      $\mathbf{h}_{i,\mathcal{B}_{pri}}^{(t)} = \mathbf{h}_{i,\mathcal{A}_{ext}}^{(t)}, v_{i,\mathcal{B}_{pri}}^{(t)} = v_{i,\mathcal{A}_{ext}}^{(t)}$.
      Message passing as **Step 1-4** in section IV-C.
      Update $\mathbf{h}_{i,\mathcal{B}_{post}}^{(t)}$ and $v_{i,\mathcal{B}_{post}}^{(t)}$ in (36).
      Update $\mathbf{h}_{i,\mathcal{B}_{ext}}^{(t)}$ and $v_{i,\mathcal{B}_{ext}}^{(t)}$ in (38).
    End While
    $\hat{\mathbf{h}}_i^{(t)} = \mathbf{h}_{i,\mathcal{B}_{ext}}^{(t)}$.
    $\boldsymbol{\Omega}^{(t)}(i) = \underset{(m,n)}{argmax}\left(\hat{\mathbf{h}}_i^{(t)}\right)$.
  End Par-For
  Combine channel as equation (39).
End When

IV. THz Sparse Channel Tracking

This section outlines the four parts of our proposed hybrid channel tracking method. First, we introduce the CSMP method to obtain the initial clustered CSI and deterministic support in part.A. Then in part.B, We describe the main modules of the VCS-TAMP channel tracking algorithm, followed by explaining the message-passing procedure in part.C. The whole above process is summarized in Algorithm 2.

A. Initial Clustering CSI Obtaining

The CSMP algorithm is based on the SP method and works by first projecting cluster residuals onto the measurement matrix and then calculating the correlation as:

$$\mathbf{e}^{(k)} = \boldsymbol{\Phi}^H \mathbf{r}^{(k)}, \tag{26}$$

$$p\left(\boldsymbol{\chi}_i^{(t)}\right) = p\left(\boldsymbol{\chi}_i^{(1,\epsilon_\chi)}\right) \prod_{m=\epsilon_\chi+1}^{2\epsilon_\chi+1} p\left(\boldsymbol{\chi}_i^{(1,m)} | \boldsymbol{\chi}_i^{(1,m-1)}\right) \prod_{m=\epsilon_\chi-1}^{1} p\left(\boldsymbol{\chi}_i^{(1,m)} | \boldsymbol{\chi}_i^{(1,m+1)}\right) \times \prod_{t=2}^{T} \left[p\left(\boldsymbol{\chi}_i^{(t,\epsilon_\chi)}\right) \prod_{m=\epsilon_\chi+1}^{2\epsilon_\chi+1} p\left(\boldsymbol{\chi}_i^{(t,m)} \middle| \boldsymbol{\chi}_i^{(t-1,m-1)}, \boldsymbol{\chi}_i^{(t,m-1)}\right) \prod_{m=\epsilon_\chi-1}^{1} p\left(\boldsymbol{\chi}_i^{(t,m)} \middle| \boldsymbol{\chi}_i^{(t-1,m+1)}, \boldsymbol{\chi}_i^{(t,m+1)}\right) \right]. \tag{22}$$

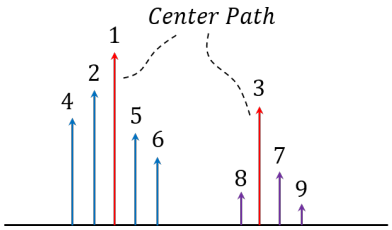

Fig. 3. Descending order of channel power with cluster distribution.

where superscript $(\cdot)^{(k)}$ is the iteration round in algorithm. After this, matched atoms are then combined to determine channel support as:

$$\mathbf{I}' = \mathbf{I}^{(k-1)} \cup \mathbf{argmax}\left(\mathbf{e}^{(k)}, \left[N_{l_1}, \cdots, N_{l_{N_i}}\right]\right), \tag{27}$$

where $\mathbf{I}$ is the channel support, $\mathbf{argmax}$ here is the function to take the largest N_{l_i} atoms in all column vector of $\mathbf{e}$. These atoms are then reevaluated using the LS descending rule:

$$\mathbf{I}^{(k)} = \mathbf{argmax}\left(\left(\mathbf{\Phi}_{\mathbf{I}'}^H \mathbf{\Phi}_{\mathbf{I}'}\right)^{-1} \mathbf{\Phi}_{\mathbf{I}'} \mathbf{y}^{(t)}, N_c\right), \tag{28}$$

where N_c is the sparsity level and represents the total number of paths to be estimated.

After the selection process, atoms are grouped into different clusters based on the descending power as Fig.3. Because we define the highest power path as the center path in a cluster, each atom must either become a new cluster center or join an existing cluster as depicted when we cluster them in descending order of power. Considering the properties mentioned above, the first highest-power atom is always selected as a cluster center and added into $\mathbf{\Omega}^{(t)}$. For the following ones, if it satisfies the conditions:

$$\min_i \quad |(m,n) - \mathbf{\Omega}^{(t)}(i)| \leq (\epsilon_\tau, \epsilon_\theta), \tag{29}$$

where (m,n) is the elements in transformed $\mathbf{I}$, the path is labeled with cluster $\mathbf{\Omega}^{(t)}$. Otherwise, the support is seen as a new cluster center and will be added into $\mathbf{\Omega}^{(t)}(i)$ as well. Therefore, all estimated paths will have corresponding labels after this fast clustering. Based on different labels, channel support $\mathbf{I}^{(k)}$ is separated into different cluster channel support, which is denoted as $\left[\mathbf{I}_1^{(k)}, \cdots, \mathbf{I}_{N_i}^{(k)}\right]$. Therefore, the i-th cluster channel is calculated as:

$$\mathbf{h}_i^{(k)} = \left(\mathbf{\Phi}_{\mathbf{I}_i}^H \mathbf{\Phi}_{\mathbf{I}_i}\right)^{-1} \mathbf{\Phi}_{\mathbf{I}_i} \mathbf{y}^{(t)}. \tag{30}$$

Though cluster channel $\left[\mathbf{h}_1^{(k)}, \cdots, \mathbf{h}_{N_i}^{(k)}\right]$ have been estimated, obtaining cluster residual $\mathbf{r}_i$ still needs the complementary techniques. Complementary support of $\mathbf{I}_i$ is $\mathbf{I}_c = \mathbf{I}^{(k)} \backslash \mathbf{I}_i^{(k)}$ and complementary channel $\mathbf{h}_c^{(k)}$ is estimated as:

$$\mathbf{h}_c^{(k)} = \left(\mathbf{\Phi}_{I_c}^H \mathbf{\Phi}_{I_c}\right)^{-1} \mathbf{\Phi}_{I_c} \mathbf{y}^{(t)}. \tag{31}$$

Once obtaining the complementary channel, we can restore the remaining cluster received signal $\mathbf{y}_i^{(k)} = \mathbf{y}^{(t)} - \mathbf{\Phi}_{\mathbf{I}_c} \mathbf{h}_c^{(k)}$ with the cluster residual $\mathbf{r}_i^{(k)} = \mathbf{y}_i^{(k)} - \mathbf{\Phi}_{\mathbf{I}_i} \mathbf{h}_i^{(k)}$ in the next iteration. And then we can obtain the labeled estimated channel.

Algorithm 3 Clustering Subspace Matching Pursuit

INPUT: $\mathbf{y}^{(t)}$, $\mathbf{\Phi}$, N_c, $\epsilon_\tau, \epsilon_\theta$.
OUTPUT: estimated labeled channel $\hat{\mathbf{h}}^{(t)}$, center path support $\mathbf{\Omega}^{(t)}$.
Initialization: $\mathbf{r}^{(1)} = \mathbf{y}, \mathbf{I} = \emptyset, \mathbf{I}_c = \emptyset, N_i = 1, k = 1$.
While $\mathbf{r}$ not uniform converge **Do**:
  $\mathbf{e}^{(k)} = \mathbf{\Phi}^H \mathbf{r}^{(k)}$.
  Update channel support $\mathbf{I}^{(k)}$ through (27) and (28).
  $\left[\mathbf{m}^{(k)}, \mathbf{n}^{(k)}\right] = \left[mod(\mathbf{I}^{(k)}, N_s), mod(\mathbf{I}^{(k)}/N_s, N_r)\right]$.
  For $(m,n) \in \left[\mathbf{m}^{(k)}, \mathbf{n}^{(k)}\right]$
    If equation (29) holds: Label $\hat{\mathbf{h}}^{(t)}$ with $\mathbf{\Omega}^{(t)}(i)$.
    Else: Append element (m,n) to vector $\mathbf{\Omega}^{(t)}$.
  End For
  Update $N_i^{(k)}$, $[N_{l_1}^{(k)}, \cdots, N_{l_{N_i}}^{(k)}]$ through channel labels.
  Obtain cluster support $[\mathbf{I}_1^{(k)}, \cdots, \mathbf{I}_{N_i}^{(k)}]$ through labels.
  For $i = 1 : N_i$
    $\mathbf{I}_c = \mathbf{I}^{(k)} \setminus \mathbf{I}_i^{(k)}$
    $\mathbf{h}_c^{(k)} = \left(\mathbf{\Phi}_{I_c}^H \mathbf{\Phi}_{I_c}\right)^{-1} \mathbf{\Phi}_{I_c} \mathbf{y}^{(t)}$
    $\mathbf{y}_i^{(k)} = \mathbf{y}^{(t)} - \mathbf{\Phi}_{I_c} \mathbf{h}_c^{(k)}$
    $\mathbf{h}_i^{(k)} = \left(\mathbf{\Phi}_{I_i}^H \mathbf{\Phi}_{I_i}\right)^{-1} \mathbf{\Phi}_{I_i} \mathbf{y}^{(y)}$
    $\mathbf{r}_i^{(k)} = \mathbf{y}_i^{(k)} - \mathbf{\Phi}_{I_i} \mathbf{h}_i^{(k)}$
  End For
  $k = k + 1$
  $\mathbf{r}^{(k)} = \left[\mathbf{r}_1^{(k)}, \cdots, \mathbf{r}_{N_i}^{(k)}\right]$
End While
For $i = 1 : N_i$
  $\hat{\mathbf{h}}^{(t,\mathbf{m},\mathbf{n})} = \mathbf{h}_i^{(k)}, \quad (m,n) \in \mathbf{I}^{(k)}$
End For

Considering the minor alterations in the subspace channel, the probability transfer parameters $q_{\boldsymbol{\chi}_i, S/T}^{0/1 \to 1/0}$ in the subsequent message passing stage can be trained using the EM method. However, we focus on channel tracking in this paper and the detailed training methods can be found in reference [16].

B. Main Modules of VCS-TAMP

The proposed VCS-TAMP algorithm comprises two essential modules, module $\mathcal{A}$ and $\mathcal{B}$, which are presented in Figure 4. Module $\mathcal{A}$ shrinks the codebook space and acts as a subspace LMMSE estimator, forwarding the estimated value and variance to module $\mathcal{B}$. Module $\mathcal{B}$ uses the structured prior on the DA domain to evolve the channel towards a sparser form and pass the message back to module $\mathcal{A}$. These loops are executed for all clusters, which create several turbo-type estimators to ensure that all subspace channels converge. After achieving convergence for all subspace channels, these estimated results are combined to generate the final tracking channel.

1) Module $\mathcal{A}$ LMMSE Estimation: Once obtaining $\mathbf{\Omega}^{(t)}$, different cluster subspaces $\mathbf{S}_i$ is established as equation (9). According to reference [15], the subspace codebook is presented as:

$$\mathbf{\Phi}_i = \mathbf{\Phi}\left(:, m + (n-1) \times \epsilon_\tau\right), (m,n) \in \mathbf{S}_i. \tag{32}$$

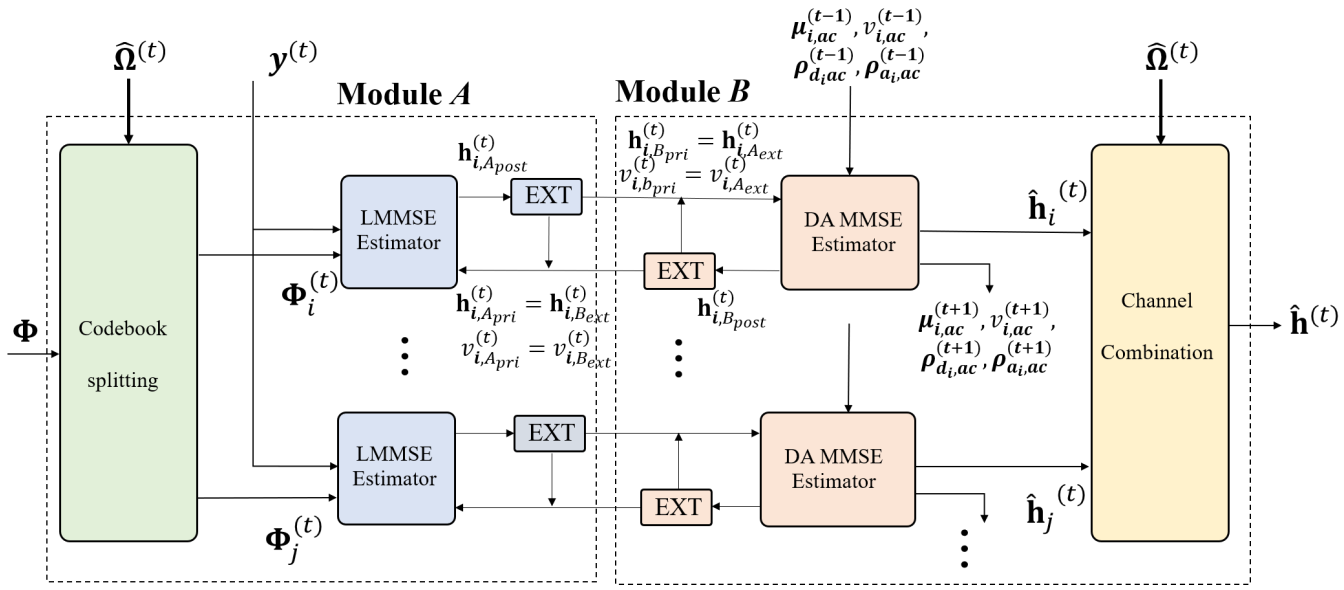

Fig. 4. Modules of the proposed VCS-AMP algorithm.

The subspace LMMSE result is given as[1]:

$$\begin{aligned}\mathbf{h}_{i,\mathcal{A}_{post}}^{(t)} &= \mathbf{h}_{i,\mathcal{A}_{pri}}^{(t)} + \frac{v_{i,\mathcal{A}_{pri}}^{(t)}}{v_{i,\mathcal{A}_{pri}}^{(t)} + \sigma_e}\mathbf{\Phi}_i^H\left(\mathbf{y}^{(t)} - \mathbf{\Phi}_i\mathbf{h}_{i,\mathcal{A}_{pri}}^{(t)}\right),\\ v_{i,\mathcal{A}_{post}}^{(t)} &= v_{i,\mathcal{A}_{pri}}^{(t)} - \frac{N_{RF}N_s}{(2\epsilon_\tau+1)(2\epsilon_\theta+1)}\frac{v_{i,\mathcal{A}_{pri}}^{(t)}}{v_{i,\mathcal{A}_{pri}}^{(t)} + \sigma_e}.\end{aligned} \tag{33}$$

And the relationship between the posterior and the prior is as:

$$\begin{aligned}&\mathcal{CN}(\hat{\mathbf{h}}^{(t)}, \mathbf{h}_{\mathcal{A}_{post}}^{(t)}, v_{\mathcal{A}_{post}}^{(t)})\\ &\quad\propto \mathcal{CN}(\hat{\mathbf{h}}^{(t)}, \mathbf{h}_{\mathcal{A}_{pri}}^{(t)}, v_{\mathcal{A}_{pri}}^{(t)})\cdot\mathcal{CN}(\hat{\mathbf{h}}^{(t)}, \mathbf{h}_{\mathcal{A}_{ext}}^{(t)}, v_{\mathcal{A}_{ext}}^{(t)}).\end{aligned} \tag{34}$$

After that, the extrinsic message can be calculated through:

$$\begin{aligned}\mathbf{h}_{i,\mathcal{A}_{ext}}^{(t)} &= v_{i,\mathcal{A}_{ext}}^{(t)}\left(\frac{\mathbf{h}_{i,\mathcal{A}_{post}}^{(t)}}{v_{i,\mathcal{A}_{post}}^{(t)}} - \frac{\mathbf{h}_{i,\mathcal{A}_{pri}}^{(t)}}{v_{i,\mathcal{A}_{pri}}^{(t)}}\right),\\ v_{i,\mathcal{A}_{ext}}^{(t)} &= \left(\frac{1}{v_{i,\mathcal{A}_{post}}^{(t)}} - \frac{1}{v_{i,\mathcal{A}_{pri}}^{(t)}}\right)^{-1}.\end{aligned} \tag{35}$$

2) Module $\mathcal{B}$ DA MMSE Estimator: Receiving the extrinsic mean and variance from the model $\mathcal{A}$, the input of module is with mean $\mathbf{h}_{i,\mathcal{B}_{pri}}^{(t)} = \mathbf{h}_{i,\mathcal{A}_{ext}}^{(t)}$ and variance $v_{i,\mathcal{B}_{pri}}^{(t)} = v_{i,\mathcal{A}_{ext}}^{(t)}$. In module $\mathcal{B}$, the message passing MMSE is executed by exploiting the proposed channel evolution model. Then the posterior mean and variance of each element is updated as:

$$\begin{aligned}\mathbf{h}_{i,\mathcal{B}_{post}}^{(t)} &= \int \hat{\mathbf{h}}_i^{(t)}\cdot p\left(\hat{\mathbf{h}}_i^{(t)}|\mathbf{h}_{i,\mathcal{B}_{pri}}^{(t)}\right),\\ v_{i,\mathcal{B}_{post}}^{(t)} &= Var\left(\hat{\mathbf{h}}_i^{(t)}|\mathbf{h}_{i,\mathcal{B}_{pri}}^{(t)}\right),\end{aligned} \tag{36}$$

[1]Because our goal is to obtain the estimated results rather than utilizing cluster residuals to select matched atoms. Even though $\mathbf{y}_i$ is not separated here, a robust result can still be obtained using LMMSE.

where $p\left(\hat{\mathbf{h}}_i^{(t)}|\mathbf{h}_{i,\mathcal{B}_{pri}}^{(t)}\right)$ is the conditional probability. According to the sum-product rule, the conditional probability satisfies:

$$p\left(\hat{\mathbf{h}}_i^{(t)}|\mathbf{h}_{i,\mathcal{B}_{pri}}^{(t)}\right) \propto \nu_{\boldsymbol{\pi}_i\to\boldsymbol{h}_i}^{(t)}\cdot\nu_{\boldsymbol{c}_i\to\boldsymbol{h}_i}^{(t)}. \tag{37}$$

The message $\nu_{\boldsymbol{c}_i\to\boldsymbol{h}_i}^{(t)}$ is the input message of module $\mathcal{B}$ and $\nu_{\boldsymbol{\pi}_i\to\boldsymbol{h}_i}^{(t)}$ is obtained through the message passing method whose whole procedure is summarized in next section IV-C. Then the module $\mathcal{B}$ updates the extrinsic mean and covariance that are resent to module $\mathcal{A}$ for iteration as:

$$\begin{aligned}\mathbf{h}_{i,\mathcal{B}_{ext}}^{(t)} &= v_{i,\mathcal{B}_{ext}}^{(t)}\left(\frac{\mathbf{h}_{i,\mathcal{B}_{post}}^{(t)}}{v_{i,\mathcal{B}_{post}}^{(t)}} - \frac{\mathbf{h}_{i,\mathcal{B}_{pri}}^{(t)}}{v_{i,\mathcal{B}_{pri}}^{(t)}}\right)\\ v_{i,\mathcal{B}_{ext}}^{(t)} &= \left(\frac{1}{v_{i,\mathcal{B}_{post}}^{(t)}} - \frac{1}{v_{i,\mathcal{B}_{pri}}^{(t)}}\right)^{-1}.\end{aligned} \tag{38}$$

When all subspace channels where $i = 1,\cdots,N_i$ get tracked, the different subspace channels are combined as:

$$\hat{\mathbf{h}}^{(t,\mathbf{m},\mathbf{n})} = \hat{\mathbf{h}}_i^{(t)}, \quad (m,n)\in\mathbf{S}_i. \tag{39}$$

C. Message Passing in VCS-TAMP

As the factor graph shown in Fig.5, the message passing procedure is divided into four main steps to obtain $\nu_{\boldsymbol{\pi}_i\to\boldsymbol{h}_i}^{(t)}$.

*1) **Step 1** (Message passing to value factor):* First, the message follows the path $\mathbf{h}_{i,\mathcal{B}_{pri}}^{(t)}\to\mathbf{c}_i^{(t)}\to\hat{\mathbf{h}}_i^{(t)}\to\boldsymbol{\pi}_i^{(t)}\to\mathbf{v}_i^{(t)}$. Without additional node, the exact message passed to value variable node $\nu_{\boldsymbol{\pi}_i\to\mathbf{v}_i}^{(t)}$ is:

$$\begin{aligned}\nu_{\boldsymbol{\pi}_i\to\mathbf{v}_i}^{(t)} = \boldsymbol{\rho}_{i,out}^{(t)}\cdot&\mathcal{CN}\left(\mathbf{v}_i^{(t)}, \mathbf{h}_{i,\mathcal{B}_{pri}}^{(t)}, v_{i,\mathcal{B}_{pri}}^{(t)}\right)\\ &+\left[1-\boldsymbol{\rho}_{i,out}^{(t)}\right]\cdot\mathcal{CN}\left(0, \mathbf{h}_{i,\mathcal{B}_{pri}}^{(t)}, v_{i,\mathcal{B}_{pri}}^{(t)}\right),\end{aligned} \tag{40}$$

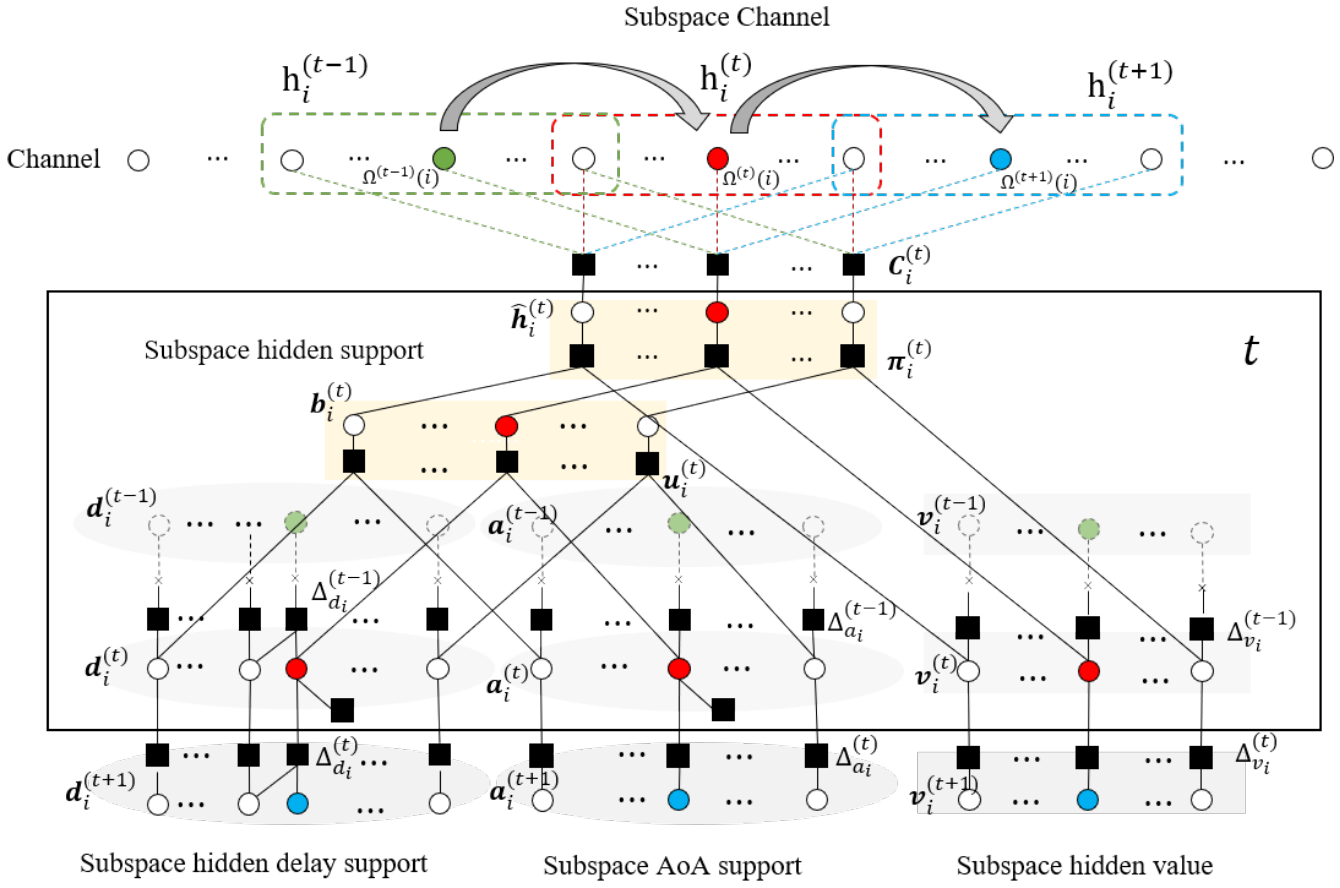

Fig. 5. Factor graph in the module $\mathcal{B}$ message passing procedure.

where $\boldsymbol{\rho}_{i,out}^{(t)}$ is the out possibility from node $\boldsymbol{\pi}_i^{(t)}$. But because the value element becomes invisible when its support is zero, this message is modified for the next effect passing according to reference [18] as:

$$\nu_{\boldsymbol{\pi}_i \to \mathbf{v}_i}^{(t)} = \mathcal{CN}\left(\mathbf{v}_i^{(t)}, \boldsymbol{\mu}_{i,in}^{(t)}, v_{i,in}^{(t)}\right), \tag{41}$$

where the mean and variance satisfy the power threshold constraint:

$$\left(\boldsymbol{\mu}_{i,in}^{(t)}, v_{i,in}^{(t)}\right) = \begin{cases} \left(\frac{1}{\epsilon}\mathbf{h}_{i,\mathcal{B}_{pri}}^{(t)}, \frac{1}{\epsilon^2}v_{i,\mathcal{B}_{pri}}^{(t)}\right), \boldsymbol{\rho}_{i,out}^{(t)} < Th, \\ \left(\mathbf{h}_{i,\mathcal{B}_{pri}}^{(t)}, v_{i,\mathcal{B}_{pri}}^{(t)}\right), \boldsymbol{\rho}_{i,out}^{(t)} \geq Th. \end{cases} \tag{42}$$

where ϵ is a small value close to zero. When the output possibility is low, the large variance makes the message at this time slot blocked as:

$$\begin{aligned} \boldsymbol{\mu}_{i,ac}^{(t+1)} &= (1-\beta)\left(\frac{v_{i,in}^{(t)} \cdot v_{i,ac}^{(t)}}{v_{i,in}^{(t)} + v_{i,ac}^{(t)}}\right)\left(\frac{\boldsymbol{\mu}_{i,ac}^{(t)}}{v_{i,ac}^{(t)}} + \frac{\boldsymbol{\mu}_{i,in}^{(t)}}{v_{i,in}^{(t)}}\right) + \beta\bar{\boldsymbol{\mu}}_i, \\ v_{i,ac}^{(t+1)} &= (1-\beta)^2\left(\frac{v_{i,in}^{(t)} \cdot v_{i,ac}^{(t)}}{v_{i,in}^{(t)} + v_{i,ac}^{(t)}}\right) + \beta^2 w^2. \end{aligned} \tag{43}$$

and the output message passed to the next time slot is almost the same as the more confident previous message. As this process is executed in all time slots, the message passed back to the node $\boldsymbol{\pi}_i^{(t)}$ is:

$$\nu_{\boldsymbol{\pi}_i \to \mathbf{v}_i}^{(t)} = \mathcal{CN}\left(\mathbf{v}_i^{(t)}, \boldsymbol{\mu}_{i,ac}^{(t)}, v_{i,ac}^{(t)}\right). \tag{44}$$

*2) **Step 2** (Message passing to delay support):* After that, the message is passed over the path $\boldsymbol{\pi}_i^{(t)} \to \mathbf{b}_i^{(t)} \to \mathbf{u}_i^{(t)} \to \mathbf{d}_i^{(t)}$ to use the delay Markov sparse structure.

• The message $\nu_{\mathbf{h}_i \to \boldsymbol{\pi}_i}^{(t)}$ is combined with a dynamic message from time slot $(t-1)$ and the message from factor node $\boldsymbol{\pi}_i$ to variable node $\mathbf{b}_i$ is as:

$$\nu_{\boldsymbol{\pi}_i \to \mathbf{b}_i}^{(t)} = \boldsymbol{\rho}_{\mathbf{b}_i,in}^{(t)} \cdot \delta\left(\mathbf{b}_i^{(t)} - 1\right) + \left(1 - \boldsymbol{\rho}_{\mathbf{b}_i,in}^{(t)}\right) \cdot \delta\left(\mathbf{b}_i^{(t)}\right), \tag{45}$$

where

$$\boldsymbol{\rho}_{\mathbf{b}_i,in}^{(t)} = \left(1 + \frac{\mathcal{CN}\left(0, \mathbf{h}_{i,\mathcal{B}_{pri}}^{(t)}, v_{i,\mathcal{B}_{pri}}^{(t)}\right)}{\mathcal{CN}\left(0, \mathbf{h}_{i,\mathcal{B}_{pri}}^{(t)} - \boldsymbol{\mu}_{i,ac}^{(t)}, v_{i,\mathcal{B}_{pri}}^{(t)} + v_{i,ac}^{(t)}\right)}\right)^{-1}. \tag{46}$$

• Because no other input message, the message $\nu_{\mathbf{b}_i \to \mathbf{u}_i}^{(t)}$ is same as received one $\nu_{\boldsymbol{\pi}_i \to \mathbf{b}_i}^{(t)}$.

• The message passed from the factor node to the delay support node needs to transform the message into a reduced-dimension delay message. So the received message node here is denoted with matrix $\mathbf{D}_i^{(t)} \in \mathbb{C}^{(2\epsilon_\tau+1)\times(2\epsilon_\theta+1)}$ as:

$$\nu_{\mathbf{u}_i \to \mathbf{D}_i}^{(t)} = \boldsymbol{\rho}_{\mathbf{D}_i,in}^{(t)} \cdot \delta\left(\mathbf{D}_i^{(t)} - 1\right) + \left(1 - \boldsymbol{\rho}_{\mathbf{D}_i,in}^{(t)}\right) \cdot \delta\left(\mathbf{D}_i^{(t)}\right), \tag{47}$$

$$\boldsymbol{\gamma}_{\boldsymbol{\chi}_i,f}^{(t,m\pm1)}=\frac{q_{\boldsymbol{\chi}_i,S}^{0\to1}\boldsymbol{\rho}_{\boldsymbol{\chi}_i,in}^{(t,m)}\boldsymbol{\gamma}_{\boldsymbol{\chi}_i,f}^{(t,m)}+q_{\boldsymbol{\chi}_i,S}^{1\to1}\left[1-\boldsymbol{\rho}_{\boldsymbol{\chi}_i,in}^{(t,m)}\right]\left[1-\boldsymbol{\gamma}_{\boldsymbol{\chi}_i,f}^{(t,m)}\right]}{\boldsymbol{\rho}_{\boldsymbol{\chi}_i,in}^{(t,m)}\boldsymbol{\gamma}_{\boldsymbol{\chi}_i,f}^{(t,m)}+\left[1-\boldsymbol{\rho}_{\boldsymbol{\chi}_i,in}^{(t,m)}\right]\left[1-\boldsymbol{\gamma}_{\boldsymbol{\chi}_i,f}^{(t,m)}\right]}, \tag{50}$$

$$\boldsymbol{\gamma}_{\boldsymbol{\chi}_i,b}^{(t,m\pm1)}=\frac{q_{\boldsymbol{\chi}_i,S}^{1\to0}\left[1-\boldsymbol{\rho}_{\boldsymbol{\chi}_i,in}^{(t,m)}\right]\left[1-\boldsymbol{\gamma}_{\boldsymbol{\chi}_i,f}^{(t,m)}\right]+\left(1-q_{\boldsymbol{\chi}_i,S}^{1\to0}\right)\boldsymbol{\rho}_{\boldsymbol{\chi}_i,in}^{(t,m)}\boldsymbol{\gamma}_{\boldsymbol{\chi}_i,f}^{(t,m)}}{\left(q_{\boldsymbol{\chi}_i,S}^{0\to0}+q_{\boldsymbol{\chi}_i,S}^{1\to0}\right)\left[1-\boldsymbol{\rho}_{\boldsymbol{\chi}_i,in}^{(t,m)}\right]\left[1-\boldsymbol{\gamma}_{\boldsymbol{\chi}_i,f}^{(t,m)}\right]+\left(q_{\boldsymbol{\chi}_i,s}^{1\to1}+q_{\boldsymbol{\chi}_i,s}^{0\to1}\right)\boldsymbol{\rho}_{\boldsymbol{\chi}_i,in}^{(t,m)}\boldsymbol{\gamma}_{\boldsymbol{\chi}_i,f}^{(t,m)}}, \tag{51}$$

$$\boldsymbol{\gamma}_{\boldsymbol{\chi}_i,f}^{(t,m\pm1)}=\frac{q_{\boldsymbol{\chi}_i,ST}^{(1,1)\to1}\boldsymbol{\rho}_{\boldsymbol{\chi}_i,ac}^{(t,m\pm1)}+q_{\boldsymbol{\chi}_i,ST}^{(1,0)\to1}\left[1-\boldsymbol{\rho}_{\boldsymbol{\chi}_i,ac}^{(t,m\pm1)}\right]}{1+\left[\left(\boldsymbol{\rho}_{\boldsymbol{\chi}_i,in}^{(t,m)}\right)^{-1}-1\right]\left[\left(\boldsymbol{\gamma}_{\boldsymbol{\chi}_i,f}^{(t,m)}\right)^{-1}-1\right]}+\frac{q_{\boldsymbol{\chi}_i,ST}^{(0,1)\to1}\boldsymbol{\rho}_{\boldsymbol{\chi}_i,ac}^{(t,m\pm1)}+q_{\boldsymbol{\chi}_i,ST}^{(1,0)\to0}\left(1-\boldsymbol{\rho}_{\boldsymbol{\chi}_i,ac}^{(t,m\pm1)}\right)}{1+\left\{\left[\left(\boldsymbol{\rho}_{\boldsymbol{\chi}_i,in}^{(t,m)}\right)^{-1}-1\right]\left[\left(\boldsymbol{\gamma}_{\boldsymbol{\chi}_i,f}^{(t,m)}\right)^{-1}-1\right]\right\}^{-1}}, \tag{52}$$

$$\gamma_{\boldsymbol{\chi}_i}^{temp\pm}=\frac{\left[1-\boldsymbol{\rho}_{\boldsymbol{\chi}_i,in}^{(t,m)}-\boldsymbol{\gamma}_{\boldsymbol{\chi}_i,b}^{(t,m)}\right]\left[q_{\boldsymbol{\chi}_i,ST}^{(0,1)\to1}\boldsymbol{\rho}_{\boldsymbol{\chi}_i,ac}^{(t,m\pm1)}+q_{\boldsymbol{\chi}_i,ST}^{(0,0)\to1}\left(1-\boldsymbol{\rho}_{\boldsymbol{\chi}_i,ac}^{(t,m\pm1)}\right)\right]+\boldsymbol{\rho}_{\boldsymbol{\chi}_i,ac}^{(t,m\pm1)}\boldsymbol{\gamma}_{\boldsymbol{\chi}_i,b}^{(t,m)}}{\left[1-\boldsymbol{\rho}_{\boldsymbol{\chi}_i,in}^{(t,m)}-\boldsymbol{\gamma}_{\boldsymbol{\chi}_i,b}^{(t,m)}\right]\left[q_{\boldsymbol{\chi}_i,ST}^{(1,0)\to0}\boldsymbol{\rho}_{\boldsymbol{\chi}_i,ac}^{(t,m\pm1)}+q_{\boldsymbol{\chi}_i,ST}^{(0,0)\to1}\left(1-\boldsymbol{\rho}_{\boldsymbol{\chi}_i,ac}^{(t,m\pm1)}\right)\right]+\boldsymbol{\rho}_{\boldsymbol{\chi}_i,ac}^{(t,m\pm1)}\boldsymbol{\gamma}_{\boldsymbol{\chi}_i,b}^{(t,m)}}, \tag{53}$$

$$\boldsymbol{\rho}_{\boldsymbol{\chi}_i,ac}^{(t+1,m,n)}=\frac{\boldsymbol{\gamma}_{\boldsymbol{\chi}_i,f}^{(t,m,n)}\boldsymbol{\gamma}_{\boldsymbol{\chi}_i,b}^{(t,m,n)}\boldsymbol{\rho}_{\boldsymbol{\chi}_i,in}^{(t,m,n)}}{\boldsymbol{\gamma}_{\boldsymbol{\chi}_i,f}^{(t,m,n)}\boldsymbol{\gamma}_{\boldsymbol{\chi}_i,b}^{(t,m,n)}\boldsymbol{\rho}_{\boldsymbol{\chi}_i,in}^{(t,m,n)}+\left[1-\boldsymbol{\gamma}_{\boldsymbol{\chi}_i,f}^{(t,m,n)}\right]\left[1-\boldsymbol{\gamma}_{\boldsymbol{\chi}_i,b}^{(t,m,n)}\right]\left[1-\boldsymbol{\rho}_{\boldsymbol{\chi}_i,in}^{(t,m,n)}\right]}, \tag{54}$$

$$\boldsymbol{\rho}_{\mathbf{A}_i,in}^{(t,m,n)}=\frac{\gamma_{\mathbf{b}_i}^{(t)}\boldsymbol{\rho}_{\mathbf{b}_i,in}^{(t,m,n)}\boldsymbol{\rho}_{\mathbf{D}_i,out}^{(t,m,n)}+\left[1-\gamma_{\mathbf{b}_i}^{(t)}\right]\left[1-\boldsymbol{\rho}_{\mathbf{b}_i,in}^{(t,m,n)}\right]\boldsymbol{\rho}_{\mathbf{D}_i,out}^{(t,m,n)}+\left[1-\boldsymbol{\rho}_{\mathbf{b}_i,in}^{(t,m,n)}\right]\left[1-\boldsymbol{\rho}_{\mathbf{D}_i,out}^{(t,m,n)}\right]}{\gamma_{\mathbf{b}_i}^{(t)}\boldsymbol{\rho}_{\mathbf{b}_i,in}^{(t,m,n)}\boldsymbol{\rho}_{\mathbf{D}_i,out}^{(t,m,n)}+\left[1-\gamma_{\mathbf{b}_i}^{(t)}\right]\left[1-\boldsymbol{\rho}_{\mathbf{b}_i,in}^{(t,m,n)}\right]\boldsymbol{\rho}_{\mathbf{D}_i,out}^{(t,m,n)}+\left[1-\boldsymbol{\rho}_{\mathbf{b}_i,in}^{(t,m,n)}\right]\left[1-\boldsymbol{\rho}_{\mathbf{D}_i,out}^{(t,m,n)}\right]+\left[1-\boldsymbol{\rho}_{\mathbf{b}_i,in}^{(t,m,n)}\right]}. \tag{55}$$

where $\boldsymbol{\rho}_{\mathbf{D}_i,in}^{(t)}=\frac{\boldsymbol{\rho}_{\mathbf{D}_i,tmp}^{(t)}}{1+\boldsymbol{\rho}_{\mathbf{D}_i,tmp}^{(t)}-\boldsymbol{\rho}_{\mathbf{b}_i}^{(t)}}$, with parameter

$$\begin{aligned}\boldsymbol{\rho}_{\mathbf{D}_i,tmp}^{(t)}=&\boldsymbol{\gamma}_{\boldsymbol{b}_i}^{(t)}\boldsymbol{\rho}_{\boldsymbol{b}_i,in}^{(t)}\boldsymbol{\rho}_{\boldsymbol{A}_i,out}^{(t)}+\left(1-\boldsymbol{\gamma}_{\boldsymbol{b}_i}^{(t)}\right)\left(1-\boldsymbol{\rho}_{\mathbf{b}_i,in}^{(t)}\right)\\&\cdot\boldsymbol{\rho}_{\mathbf{A}_i,out}^{(t)}+\left(1-\boldsymbol{\rho}_{\mathbf{b}_i,in}^{(t)}\right)\left(1-\boldsymbol{\rho}_{\mathbf{A}_i,out}^{(t)}\right).\end{aligned} \tag{48}$$

Then $\boldsymbol{\rho}_{\mathbf{D}_i,in}^{(t)}$ is transformed to $\boldsymbol{\rho}_{\mathbf{d}_i,in}^{(t)}$ through summing different element with same delay support mark:

$$\boldsymbol{\rho}_{\mathbf{d}_i,in}^{(t,m)}=\frac{\prod_n\boldsymbol{\rho}_{\mathbf{D}_i,in}^{(t,m,n)}}{\prod_n\boldsymbol{\rho}_{\mathbf{D}_i,in}^{(t,m,n)}+\prod_n\left(1-\boldsymbol{\rho}_{\mathbf{D}_i,in}^{(t,m,n)}\right)}. \tag{49}$$

Therefore, the message passed to the delay support variable node is $\nu_{\mathbf{u}_i\to\mathbf{d}_i}^{(t)}=\boldsymbol{\rho}_{\mathbf{d}_i,in}^{(t)}$.

• So we can update the delay support message $\boldsymbol{\rho}_{\mathbf{d}_i,out}^{(t)}$ according aforementioned subspace statistical channel evolution model with substituting the $\mathbf{d}_i$ into temp notation $\boldsymbol{\chi}_i$, which is summarized as Algorithm 4, where the related equation is in (50)-(53).

• After calculating the forward and backward passing message, the message passed to the delay support message next time slot is:

$$\nu_{\mathbf{d}_i\to\boldsymbol{\Delta}_{\mathbf{d}_i}}^{(t+1)}=\boldsymbol{\rho}_{\boldsymbol{\chi}_i,ac}^{(t)}\delta\left(\mathbf{d}_i^{(t)}-1\right)+\left(1-\boldsymbol{\rho}_{\mathbf{d}_i,ac}^{(t)}\right)\delta\left(\mathbf{d}_i^{(t)}\right), \tag{56}$$

where $\boldsymbol{\rho}_{\mathbf{d}_i,ac}^{(t+1)}$ is obtained in equation (54) with substituting the $\mathbf{d}_i$ into $\boldsymbol{\chi}_i$ as well.

*3) **Step 3** (Message passing to AoA support):* The message backtrack through $\mathbf{d}_i^{(t)}\to\mathbf{u}_i^{(t)}\to\mathbf{a}_i^{(t)}$ to capture the structured sparsity on AoA domain as:

• In the returning path, the reduced-dimension message will be split into higher dimensions on node $\mathbf{u}_i$ as:

$$\nu_{\boldsymbol{d}_i\to\mathbf{u}_i}^{(t)}=\boldsymbol{\rho}_{\mathbf{D}_i,out}^{(t)}\cdot\delta\left(\mathbf{D}_i^{(t)}-1\right)+\left(1-\boldsymbol{\rho}_{\mathbf{D}_i,out}^{(t)}\right)\cdot\delta\left(\mathbf{D}_i^{(t)}\right), \tag{57}$$

Algorithm 4 Subspace DA Support Estimation.

1: **INPUT**: $\boldsymbol{\rho}_{\boldsymbol{\chi}_i,in}^{(t)},\boldsymbol{\rho}_{\boldsymbol{\chi}_i,ac}^{(t)}$.
2: **OUTPUT**: $\boldsymbol{\rho}_{\boldsymbol{\chi}_i,out}^{(t)}$.
3: **When** $t=(t'+1)$:
4: $\boldsymbol{\gamma}_{\boldsymbol{\chi}_i,f}^{(t,\epsilon_\chi)}=\gamma_c$; $\boldsymbol{\gamma}_{\boldsymbol{\chi}_i,b}^{(t,1)}=\gamma_m$; $\boldsymbol{\gamma}_{\boldsymbol{\chi}_i,b}^{(t,2\epsilon_\tau+1)}=\gamma_m$.
5: **For** $m=\epsilon_\tau:1$, obtain $\boldsymbol{\gamma}_{\boldsymbol{\chi}_i,f}^{(t,m-1)}$ as (50).
6: **For** $m=\epsilon_\tau:2\epsilon_\tau+1$, obtain $\boldsymbol{\gamma}_{\boldsymbol{\chi}_i,f}^{(t,m+1)}$ as (50).
7: **For** $m=1:\epsilon_\tau-1$, obtain $\boldsymbol{\gamma}_{\boldsymbol{\chi}_i,b}^{(t,m+1)}$ as (51).
8: **For** $m=2\epsilon+1:\epsilon+1$, obtain $\boldsymbol{\gamma}_{\boldsymbol{\chi}_i,b}^{(t,m-1)}$ as (51).
9: **Else When** $t>(t'+1)$
10: $\boldsymbol{\gamma}_{\boldsymbol{\chi}_i,c}^{(t,\epsilon_\tau)}=q_{\boldsymbol{\chi}_i,T}^{0\to1}\left(1-\boldsymbol{\rho}_{\boldsymbol{\chi}_i}^{ac}\right)+\left(1-q_{\boldsymbol{\chi}_i,T}^{1\to0}\right)\boldsymbol{\rho}_{\boldsymbol{D}_i}^{ac}$.
11: $\boldsymbol{\gamma}_{\boldsymbol{\chi}_i,b}^{(t,1)}=0,\quad\boldsymbol{\gamma}_{\boldsymbol{\chi}_i,b}^{(t,2\epsilon_\tau+1)}=0$.
12: **For** $m=\epsilon_\tau:1$, obtain $\boldsymbol{\gamma}_{\boldsymbol{\chi}_i,f}^{(t,m-1)}$ as (52).
13: **For** $m=\epsilon_\tau:\epsilon_\tau+1$, obtain $\boldsymbol{\gamma}_{\boldsymbol{\chi}_i,f}^{(t,m+1)}$ as (52).
14: **For** $m=1:\epsilon_\tau-1$, obtain $\boldsymbol{\gamma}_{\boldsymbol{\chi}_i,f}^{(t,m+1)}=\frac{1}{1+\gamma_{\boldsymbol{\chi}_i}^{temp+}}$, where $\gamma_{\boldsymbol{\chi}_i}^{temp+}$ is as (53).
15: **For** $m=2\epsilon_\tau+1:\epsilon_\tau$, obtain $\boldsymbol{\gamma}_{\boldsymbol{\chi}_i}^{f}(t,m-1)=\frac{1}{1+\gamma_{\boldsymbol{\chi}_i}^{temp-}}$, where $\gamma_{\boldsymbol{\chi}_i}^{temp-}$ is as (53).
16: Calculates $\boldsymbol{\rho}_{\boldsymbol{\chi}_i}^{out}=\frac{\boldsymbol{\gamma}_{\boldsymbol{\chi}_i}^{f}\cdot\boldsymbol{\gamma}_{\boldsymbol{\chi}_i}^{b}}{\boldsymbol{\gamma}_{\boldsymbol{\chi}_i}^{f}\cdot\boldsymbol{\gamma}_{\boldsymbol{\chi}_i}^{b}+\left(1-\boldsymbol{\gamma}_{\boldsymbol{\chi}_i}^{f}\right)\cdot\left(1-\boldsymbol{\gamma}_{\boldsymbol{\chi}_i}^{b}\right)}$.
17: **End When**

where

$$\boldsymbol{\rho}_{\mathbf{D}_i,out}^{(t,m,n)}=\frac{\boldsymbol{\rho}_{\mathbf{d}_i,out}^{(t,m)}}{\boldsymbol{\rho}_{\mathbf{d}_i,out}^{(t,m)}+\left[1-\boldsymbol{\rho}_{\mathbf{d}_i,out}^{(t,m)}\right]\prod\limits_{n'\neq n}\left[\left(\boldsymbol{\rho}_{\mathbf{D}_i,in}^{(t,m,n)}\right)^{-1}-1\right]}. \tag{58}$$

• Then the message passed from node $\mathbf{u}_i^{(t)}$ to the AoA node $\mathbf{a}_i^{(t)}$ is as:

$$\nu_{\mathbf{u}_i\to\mathbf{a}_i}^{(t)} = \boldsymbol{\rho}_{\mathbf{A}_i,in}^{(t)} \cdot \delta\left(\mathbf{d}_i^{(t)} - 1\right) + \left(1 - \boldsymbol{\rho}_{\mathbf{A}_i,in}^{(t)}\right) \cdot \delta\left(\mathbf{d}_i^{(t)}\right), \quad (59)$$

with $\boldsymbol{\rho}_{\mathbf{A}_i,in}^{(t,m,n)}$ in (55). It is reduced again similarly as:

$$\boldsymbol{\rho}_{\mathbf{a}_i,in}^{(t,m)} = \frac{\prod_m \boldsymbol{\rho}_{\mathbf{A}_i,in}^{(t,m,n)}}{\prod_m \boldsymbol{\rho}_{\mathbf{A}_i,in}^{(t,m,n)} + \prod_m \left(1 - \boldsymbol{\rho}_{\mathbf{A}_i,in}^{(t,m,n)}\right)}. \quad (60)$$

• Then we can obtain $\boldsymbol{\rho}_{\mathbf{a}_i,out}^{(t)}$ similarly through Algorithm 4 substituting the $\mathbf{a}_i$ into temp notation $\boldsymbol{\chi}_i$. The message passed to the next time slot is:

$$\nu_{\mathbf{a}_i\to\boldsymbol{\Delta}_{\mathbf{a}_i}}^{(t+1)} = \boldsymbol{\rho}_{\mathbf{a}_i,ac}^{(t)} \delta\left(\mathbf{a}_i^{(t)} - 1\right) + \left(1 - \boldsymbol{\rho}_{\mathbf{a}_i,ac}^{(t)}\right) \delta\left(\mathbf{a}_i^{(t)}\right), \quad (61)$$

which obtains $\boldsymbol{\rho}_{\mathbf{a}_i,ac}^{(t+1)}$ through substituting the $\mathbf{a}_i$ into $\boldsymbol{\chi}_i$ in equation (54).

*4) **Step 4** (Message passed to estimated channel):* The message is finally passed back over the path $\mathbf{a}_i^{(t)} \to \mathbf{u}_i^{(t)} \to \mathbf{b}_i^{(t)} \to \boldsymbol{\pi}_i^{(t)} \to \mathbf{h}_i^{(t)}$, and the details steps are as follows:
• The message $v_{\mathbf{a}i\to\mathbf{u}_i}^{(t)} = \boldsymbol{\rho}_{\mathbf{u}_i,out}^{(t)}$ is first transformed into DA-structured form message through equation:

$$\nu_{\mathbf{a}_i\to\mathbf{u}_i}^{(t)} = \boldsymbol{\rho}_{\mathbf{A}_i,out}^{(t)} \delta\left(\mathbf{a}_i^{(t)} - 1\right) + \left(1 - \boldsymbol{\rho}_{\mathbf{A}_i,out}^{(t)}\right) \delta\left(\mathbf{a}_i^{(t)} - 1\right), \quad (62)$$

where

$$\boldsymbol{\rho}_{\mathbf{A}_i,out}^{(t,m,n)} = \frac{\boldsymbol{\rho}_{\mathbf{a}_i,out}^{(t)}}{\boldsymbol{\rho}_{\mathbf{a}_i,out}^{(t,m)} + \left[1 - \boldsymbol{\rho}_{\mathbf{a}_i,out}^{(t,m)}\right] \prod_{m'\neq m} \left[\left(\boldsymbol{\rho}_{\mathbf{A}_i,in}^{(t,m',n)}\right)^{-1} - 1\right]} \quad (63)$$

.
• And then the message is trace back to node $\mathbf{b}_i^{(t)}$ as:

$$\nu_{\mathbf{u}_i\to\mathbf{b}_i}^{(t)} = \boldsymbol{\rho}_{\mathbf{b}_i,out}^{(t)} \delta\left(\mathbf{b}_i^{(t)} - 1\right) + \left(1 - \boldsymbol{\rho}_{\mathbf{b}_i,out}^{(t)}\right) \delta\left(\mathbf{b}_i^{(t)} - 1\right), \quad (64)$$

with combined possibility $\boldsymbol{\rho}_{\mathbf{b}_i,out}^{(t,m,n)} = \boldsymbol{\rho}_{\mathbf{D}_i,out}^{(t,m,n)} \boldsymbol{\rho}_{\mathbf{A}_i,out}^{(t,m,n)} \gamma_{\mathbf{b}_i}^{(t)}$.
• Without additional message from other factors, the message passes to factor node $\pi_i^{(t)}$ is the same as the input, which is denoted as $\nu_{\mathbf{b}_i\to\boldsymbol{\pi}_i}^{(t)} = \nu_{\mathbf{u}_i\to\mathbf{b}_i}^{(t)}$.
• Finally the message is passed back to estimated node $\hat{\mathbf{h}}_i^{(t)}$, and can be denoted as:

$$\nu_{\boldsymbol{\pi}_i\to\boldsymbol{h}_i}^{(t)} = \boldsymbol{\rho}_{\mathbf{b}_i,out}^{(t)} \mathcal{CN}\left(\hat{\mathbf{h}}_i^{(t)}, \boldsymbol{\mu}_{i,ac}^{(t)}, v_{i,ac}^{(t)}\right) + \left(1 - \boldsymbol{\rho}_{\mathbf{b}_i,out}^{(t)}\right) \delta\left(\mathbf{b}_i^{(t)} - 1\right). \quad (65)$$

V. Simulation

In our simulation, the frequency is set at 300GHz to significantly distinguish THz from millimeter waves, the bandwidth is 2GHz to avoid the effect of beam splitting, and the number of antenna and RF chains are 128 and 8 respectively. The indoor dynamic channel model in reference [25] is adapted to generate the initial scattering ray of our simulation. Other simulation parameters are shown in Table.I.

TABLE I
Table of Simulation Parameters

Parameters	Values
Carrier Frequency	300 GHz
Bandwidth	2 GHz
BS Antenna Number and RF chain	(128,8)
Number Pilots	64
Channel Model	THz channel model [25]
Cluster number and inta-cluster paths	(3,1∼20)
$(\epsilon_\tau, \epsilon_\theta)$	(6,6)
N_c	40
User and Scatter Velocity	(5m/s, 2.5m/s)
Initialization and Tracking Frame	(10,1000)
Monte-Carlo Iteration	100

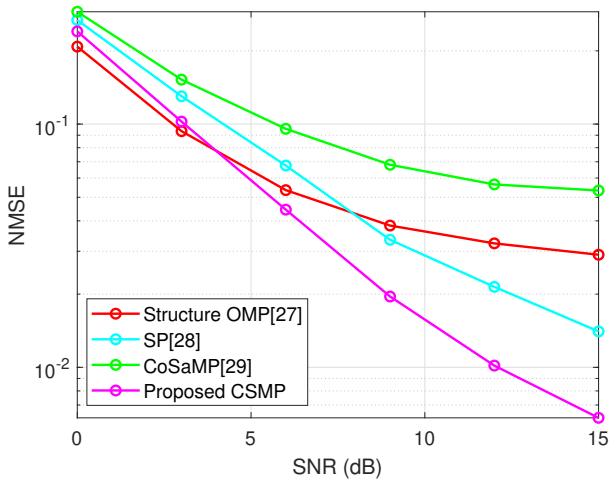

Fig. 6. The NMSE performance against the SNR in the initialization phase.

A. CSMP Performance Analysis

The main purpose is to obtain clustered CSI through channel estimation for future tracking in the initialization phase. Tracking accuracy and clustering ability are important and computation time simulation is omitted here because the initialization frame is much less than the true tracking frame. So normalized mean squared error (NMSE) is applied to compare different estimation method accuracy, and it is calculated as:

$$NMSE = \frac{\left\|\hat{\mathbf{h}}^{(t)} - \mathbf{h}^{(t)}\right\|^2}{\left\|\mathbf{h}^{(t)}\right\|^2}. \quad (66)$$

The baseline concludes some classic channel estimation methods with the same algorithm structure, greedy-series structured-OMP [28] and the classic subspace-series SP [29], CoSaMP [30] subspace algorithms of the same structure. The NMSE of different methods is presented in Fig.6. When the signal-to-noise ratio (SNR) is low, due to the inaccurate obtained clustered CSI, the advantages of our proposal are not obvious because nearly all algorithms show poor estimation performance. But when SNR gets improved, the clustered channel becomes much more accurate and CSMP can effectively maintain cluster CSI and reduce the probability of

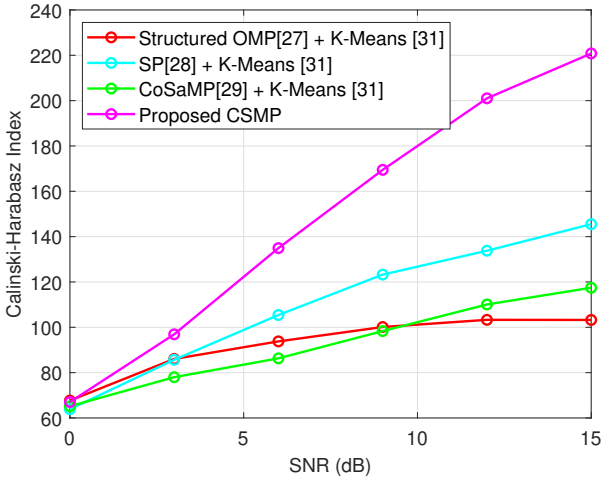

Fig. 7. The CHI performance against the SNR in the initialization phase.

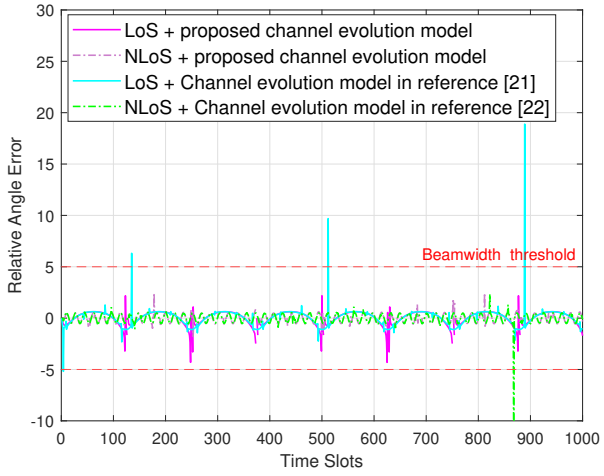

Fig. 9. Relative angle error for different evolution models under perfect CSI

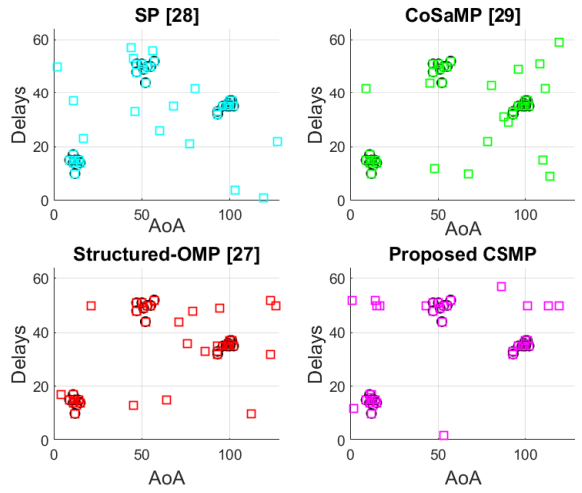

Fig. 8. Estimation result snapshot with sparsity-level 40 at SNR 15dB.

mismatches. Therefore, it can be much better NMSE when SNR is greater than 5dB.

The internal evaluation Calinski-Harabasz index (CHI) calculated as reference [31] in Fig.7 is applied to validate the clustering performance. As CHI is the ratio between inter-cluster variance and intra-cluster variation, a better clustering algorithm should have a higher CHI. The aforementioned channel estimation methods are combined with traditional K-means clustering [32] to compare with the proposed CSMP method. Consistent with the trend of NMSE performance changes against SNR, the CHI of different algorithms are almost the same when the SNR ratio is low. However, as SNR continues to increase, the CHI of the CSMP algorithm is greatly improved. A snapshot is shown in Fig.8 with a sparsity level set at 40 to more intuitively present the clustering distribution of the estimated result channel.

B. Hybrid Channel Tracking Performance Analysis

In this part, before comparing the time average NMSE (TNMSE) of different channel tracking methods, the robustness of the proposed deterministic channel evolution model is validated as Fig.9. Compared with traditional THz deterministic channel tracking study [21], [22], our proposed channel evolution model has a lower probability of link interruption under 5 degrees beamwidth given in reference [33] robust mode. In addition, our proposed DA channel variation has a smaller variance in both LoS and NLoS conditions, which is crucial for the following tracking.

The accuracy and time complexity of different THz channel tracking methods are compared. The baseline includes two ST methods and two DT methods. For the first ST methods [15], it ignores the DA-MM structure for channel evolution and assumes different channel support element is independent identical distribution (i.i.d). Another ST baseline is to modify it with 2D-MM proposed in [16]. For DT methods, we select the tracking methods in reference [21], [22] to track the channel with different LoS-only and LoS/NLoS mixed channel evolution models respectively. With all of the above baselines, we can compare our proposal with ST and DT in both model-matched or unmatched conditions.

In Fig.10, TNMSE is applied to compare the accuracy:

$$TNMSE = \frac{1}{T-t'} \sum_{t=t'+1}^{T} \frac{\left\| \hat{\mathbf{h}}^{(t)} - \mathbf{h}^{(t)} \right\|^2}{\left\| \mathbf{h}^{(t)} \right\|^2}. \tag{67}$$

It can be seen whether the model matches have a significant impact on DT compared with ST and HT. Without an effective model, DT method can not obtain effective results which is even worse than most estimation methods. This confirms the poor generalization ability of the deterministic scheme mentioned earlier, which relies on the analysis of environmental prior information. For ST having stronger generalization ability, whether model matching has a lighter impact on the tracking TNMSE performance result. The TNMSE performance of our proposed surpasses traditional ST mode originates from our segmentation of clusters subspace. Because the channels within the cluster usually have more consistent

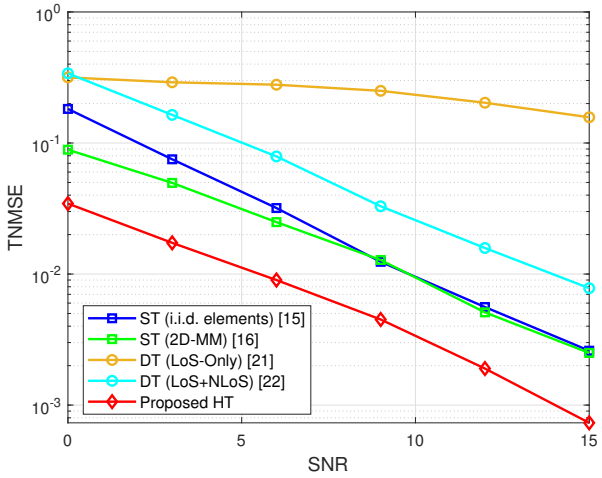

Fig. 10. The NMSE performance against the SNR in the tracking phase.

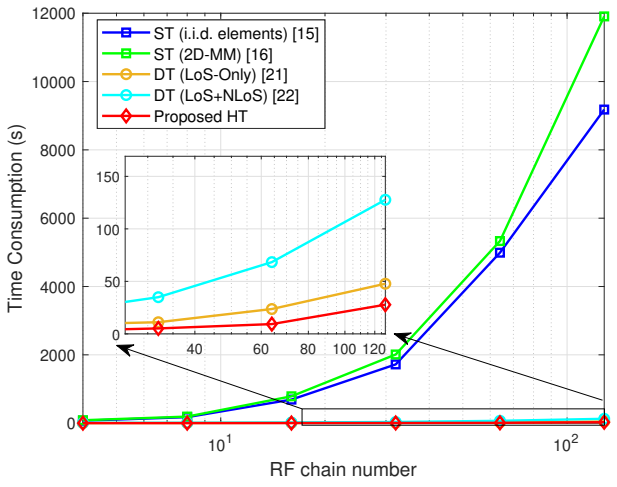

Fig. 11. Time consumption against the RF chain in the tracking phase.

statistical characteristics, the MMSE estimation variance in message passing satisfies:

$$v_i^{(t)} \ll v^{(t)}, \quad i = 1, \cdots, N_c. \tag{68}$$

This not only improves the accuracy of channel estimation greatly, but also promotes convergence time of the message passing part in HT as Fig.11.

In Fig.11, our proposed achieve amazing improvement compared with other tracking scheme, which even faster than DT method. Comparing using equations to evolve all path, fast-converging partially parameterized HT can improve systems efficiency. Besides, as different cluster channel are almost independent, the scale of the tracking problem has also been reduced to within a cluster subspace rather than the full channel which accounts for the computation performance.

In summary, our approach provides a more flexible architecture for channel tracking by combining the advantages of deterministic and statistical tracking schemes, which can achieve a good improvement in both performance and complexity.

VI. Conclusion

In this paper, we investigated the hybrid channel tracking for THz massive MIMO systems in dynamic environments. To capture the temporal correlation of the THz channel, a hybrid channel evolution model is developed based on THz channel cluster characteristics. Based on the proposed model, our hybrid channel tracking method solves the clustered CSI acquisition problem in initialization and following utilizes the cluster CSI in tracking to promote both accuracy and time consumption performance.

For details, we use complementary technology to hold the cluster information in CSMP, which achieves better estimation performance and clustering results than the traditional ones. The estimated subspace path has more consistent statistical characteristics, and VCS-TAMP can give accuracy with great promotion. Besides, VCS-TAMP greatly shrinks the codebook to subspace size, and has parallelized the traditional AMP estimation frame for the different clusters, which makes time consumption of our proposed is quite low. Analytical and numerical results have shown that the proposed achieved a superior performance than previous work. In the future, more work can be excavated, such as the combination of beam splits, near-field effects, and so on other unideal characteristics in the THz massive MIMO.

References

[1] N. Yang and A. Shafie, "Terahertz communications for massive connectivity and security in 6g and beyond era," *IEEE Commun. Mag.*, 2022.
[2] C. Chaccour, M. N. Soorki, W. Saad, M. Bennis, and P. Popovski, "Can terahertz provide high-rate reliable low-latency communications for wireless vr?" *IEEE Internet Things J.*, vol. 9, no. 12, pp. 9712–9729, 2022.
[3] Z. Zhang, Y. Xiao, Z. Ma, M. Xiao, Z. Ding, X. Lei, G. K. Karagiannidis, and P. Fan, "6g wireless networks: Vision, requirements, architecture, and key technologies," *IEEE Veh. Technol. Mag.*, vol. 14, no. 3, pp. 28–41, 2019.
[4] C. Han, W. Gao, N. Yang, and J. M. Jornet, "Molecular absorption effect: A double-edged sword of terahertz communications," *IEEE Wireless Commun.*, 2022.
[5] H. Cox, R. Zeskind, and M. Owen, "Robust adaptive beamforming," *IEEE Trans. Acoust., Speech, Signal Process.*, vol. 35, no. 10, pp. 1365–1376, 1987.
[6] B. Ning, Z. Tian, W. Mei, Z. Chen, C. Han, S. Li, J. Yuan, and R. Zhang, "Beamforming technologies for ultra-massive mimo in terahertz communications," *IEEE Open J. Commun. Soc.*, vol. 4, pp. 614–658, 2023.
[7] Y. Wang, C. Yang, Z. Ren, Y. Sun, and M. Peng, "Sensing-aided hybrid precoding for efficient terahertz wideband communications in multi-user high-data-rate iot," *IEEE Internet of Things Journal*, 2023.
[8] X. Shao, X. Chen, C. Zhong, and Z. Zhang, "Exploiting simultaneous low-rank and sparsity in delay-angular domain for millimeter-wave/terahertz wideband massive access," *IEEE Trans. Wireless Commun.*, vol. 21, no. 4, pp. 2336–2351, 2021.
[9] V. Petrov, D. Moltchanov, Y. Koucheryavy, and J. M. Jornet, "Capacity and outage of terahertz communications with user micro-mobility and beam misalignment," *IEEE Trans. Veh. Technol.*, vol. 69, no. 6, pp. 6822–6827, 2020.
[10] J. Dai, A. Liu, and V. K. Lau, "Fdd massive mimo channel estimation with arbitrary 2d-array geometry," *IEEE Trans. Signal Process.*, vol. 66, no. 10, pp. 2584–2599, 2018.
[11] C. Komninakis, C. Fragouli, A. H. Sayed, and R. D. Wesel, "Multi-input multi-output fading channel tracking and equalization using kalman estimation," *IEEE Trans. Antennas Propag.*, vol. 50, no. 5, pp. 1065–1076, 2002.
[12] M. Robaei and R. Akl, "Quadratic displacement operators—theory and application to millimeter-wave channel tracking," *IEEE Trans. Wireless Commun.*, vol. 22, no. 1, pp. 596–610, 2022.

[13] I. F. Akyildiz, C. Han, Z. Hu, S. Nie, and J. M. Jornet, "Terahertz band communication: An old problem revisited and research directions for the next decade," *IEEE Trans. Commun.*, vol. 70, no. 6, pp. 4250–4285, 2022.
[14] S. Nie and I. F. Akyildiz, "Three-dimensional dynamic channel modeling and tracking for terahertz band indoor communications," in *2017 IEEE 28th Annual International Symposium on Personal, Indoor, and Mobile Radio Communications (PIMRC)*. IEEE, 2017, pp. 1–5.
[15] J. Ma, X. Yuan, and L. Ping, "On the performance of turbo signal recovery with partial dft sensing matrices," *IEEE Signal Process. Lett.*, vol. 22, no. 10, pp. 1580–1584, 2015.
[16] L. Lian, A. Liu, and V. K. Lau, "Exploiting dynamic sparsity for downlink fdd-massive mimo channel tracking," *IEEE Trans. Signal Process.*, vol. 67, no. 8, pp. 2007–2021, 2019.
[17] J. Yu, X. Liu, Y. Gao, and X. Shen, "3d channel tracking for uav-satellite communications in space-air-ground integrated networks," *IEEE J. Sel. Areas Commun.*, vol. 38, no. 12, pp. 2810–2823, 2020.
[18] ——, "3d on and off-grid dynamic channel tracking for multiple uavs and satellite communications," *IEEE Trans. Wireless Commun.*, vol. 21, no. 6, pp. 3587–3604, 2021.
[19] X. Cheng, Z. Huang, and L. Bai, "Channel nonstationarity and consistency for beyond 5g and 6g: A survey," *IEEE Commun. Surv. Tutor.*, vol. 24, no. 3, pp. 1634–1669, 2022.
[20] J. Wang, C.-X. Wang, J. Huang, H. Wang, X. Gao, X. You, and Y. Hao, "A novel 3d non-stationary gbsm for 6g thz ultra-massive mimo wireless systems," *IEEE Trans. Veh. Technol.*, vol. 70, no. 12, pp. 12 312–12 324, 2021.
[21] X. Gao, L. Dai, Y. Zhang, T. Xie, X. Dai, and Z. Wang, "Fast channel tracking for terahertz beamspace massive mimo systems," *IEEE Trans. Veh. Technol.*, vol. 66, no. 7, pp. 5689–5696, 2016.
[22] D. Bilibashi, E. M. Vitucci, and V. Degli-Esposti, "On dynamic ray tracing and anticipative channel prediction for dynamic environments," *IEEE Trans. Antennas Propag.*, 2023.
[23] A. Liao, Z. Gao, D. Wang, H. Wang, H. Yin, D. W. K. Ng, and M.-S. Alouini, "Terahertz ultra-massive mimo-based aeronautical communications in space-air-ground integrated networks," *IEEE J. Sel. Areas Commun.*, vol. 39, no. 6, pp. 1741–1767, 2021.
[24] W. Khawaja, O. Ozdemir, and I. Guvenc, "Channel prediction for mmwave ground-to-air propagation under blockage," *IEEE Antennas Wirel. Propag. Lett.*, vol. 20, no. 8, pp. 1364–1368, 2021.
[25] Y. Chen, Y. Li, C. Han, Z. Yu, and G. Wang, "Channel measurement and ray-tracing-statistical hybrid modeling for low-terahertz indoor communications," *IEEE Trans. Wireless Commun.*, vol. 20, no. 12, pp. 8163–8176, 2021.
[26] J. Zhang, J. Lin, P. Tang, Y. Zhang, H. Xu, T. Gao, H. Miao, Z. Chai, Z. Zhou, Y. Li *et al.*, "Channel measurement, modeling, and simulation for 6g: A survey and tutorial," *arXiv preprint arXiv:2305.16616*, 2023.
[27] A. Brighente, M. Cerutti, M. Nicoli, S. Tomasin, and U. Spagnolini, "Estimation of wideband dynamic mmwave and thz channels for 5g systems and beyond," *IEEE Journal on Selected Areas in Communications*, vol. 38, no. 9, pp. 2026–2040, 2020.
[28] Y. You, L. Zhang, M. Yang, Y. Huang, X. You, and C. Zhang, "Structured omp for irs-assisted mmwave channel estimation by exploiting angular spread," *IEEE Transactions on Vehicular Technology*, vol. 71, no. 4, pp. 4444–4448, 2022.
[29] S. Haghighatshoar and G. Caire, "Low-complexity massive mimo subspace estimation and tracking from low-dimensional projections," *IEEE Transactions on Signal Processing*, vol. 66, no. 7, pp. 1832–1844, 2018.
[30] W. Shen, L. Dai, Y. Shi, B. Shim, and Z. Wang, "Joint channel training and feedback for fdd massive mimo systems," *IEEE Transactions on vehicular technology*, vol. 65, no. 10, pp. 8762–8767, 2015.
[31] U. Maulik and S. Bandyopadhyay, "Performance evaluation of some clustering algorithms and validity indices," *IEEE Transactions on pattern analysis and machine intelligence*, vol. 24, no. 12, pp. 1650–1654, 2002.
[32] T. Kanungo, D. M. Mount, N. S. Netanyahu, C. D. Piatko, R. Silverman, and A. Y. Wu, "An efficient k-means clustering algorithm: Analysis and implementation," *IEEE transactions on pattern analysis and machine intelligence*, vol. 24, no. 7, pp. 881–892, 2002.
[33] Y. Karaçora, C. Chaccour, A. Sezgin, and W. Saad, "Event-based beam tracking with dynamic beamwidth adaptation in terahertz (thz) communications," *IEEE Trans. Commun.*, 2023.

Yuheng Fan received the B.S. degree in information and communication engineering from Beijing University of Posts and Telecommunications, Beijing, China in 2023, where he is currently pursuing th Ph.D degree in information and communication engineering with the State Key Laboratory of Networking and Switching Technology. His research is interested in massive MIMO terahertz communication signal processing.

Chuang Yang (Member, IEEE) received the B.S. degree in electronic information science and technology from Chongqing University, Chongqing, China, in 2015, and the Ph.D. degree in microelectronics and solid-state electronics from Tianjin University, Tianjin, China, in 2020. He is currently an Associate Researcher with the State Key Laboratory of Networking and Switching Technology, Beijing University of Posts and Telecommunications, Beijing, China. His research interests include microwave and terahertz measurement, and terahertz integrated sensing and communication.

Yanran Sun received the B.S. degree in materials science and engineering from Beijing University of Posts and Telecommunications, Beijing, China, in 2021, where she is currently pursuing the Ph.D. degree in information and communication engineering with the State Key Laboratory of Networking and Switching Technology. Her research interests include massive MIMO and terahertz communications.

Mugen Peng (Fellow, IEEE) received the Ph.D. degree in communication and information systemss from Beijing University of Posts and Telecommunications (BUPT), Beijing, China, in 2005. Afterward, he joined BUPT, where he has been a Full Professor with the School of Information and Communication Engineering since 2012. In 2014, he was also an Academic Visiting Fellow with Princeton University, Princeton, NJ, USA. He leads a Research Group focusing on wireless transmission and networking technologies with BUPT. He has authored and coauthored over 100 refereed IEEE journal papers and over 300 conference proceeding papers. His main research areas include wireless communication theory, radio signal processing, cooperative communication, self-organization networking, heterogeneous networking, cloud communication, and Internet of Things. Prof. Peng was a recipient of the 2018 Heinrich Hertz Prize Paper Award; the 2014 IEEE ComSoc AP Outstanding Young Researcher Award; and the Best Paper Award in the ICC 2022, JCN 2016, IEEE WCNC 2015, IEEE GameNets 2014, IEEE CIT 2014, ICCTA 2011, IC-BNMT 2010, and IET CCWMC 2009. He is on the editorial/associate editorial board of the IEEE Communications Magazine, IEEE Access, the IEEE Internet of Things Journal, IET Communications, and China Communications. He is a Fellow of IET.